UNIVERSITY OF TARTU
Faculty of Science and Technology
Institute of Chemistry

Tinatin Tkesheliadze

Oxygen Reduction Catalysts Based on Iron and Cobalt Phthalocyanine Modified Shungite

Bachelor's Thesis (12 ECTS)

Curriculum Science and Technology

Supervisors:
Marek Mooste, PhD
Kaido Tammeveski, PhD

Tartu 2020

Oxygen Reduction Catalysts Based on Iron and Cobalt Phthalocyanine Modified Shungite

Abstract:

Electrocatalytic oxygen reduction reaction (ORR) activity was studied on natural shungite-based materials prepared by functionalisation with Fe- and Co-phthalocyanine (Pc) complexes via pyrolysis. Structural and elemental composition of the pristine and modified catalysts were studied using several physical characterisation methods. The ORR activity of the materials was assessed by the rotating disc electrode method in alkaline and acidic media, resulting in superior ORR performance of KOH-treated FePc modified shungite material in 0.1 M KOH solution. Stability testing performed on most active catalysts in alkaline media showed a high stability of the prepared shungite-based electrocatalysts. The testing in 0.5 M H_2SO_4 solution also revealed the superior ORR activity of KOH-treated FePc modified shungite material.

Keywords: electrocatalysis, oxygen reduction reaction, non-precious metal catalyst, shungite

CERCS: P401 Electrochemistry

Hapniku redutseerumine raud ja koobalt ftalotsüaniiniga modifitseeritud šungiidil põhinevatel katalüsaatormaterjalidel

Lühikokkuvõte:

Käesolevas töös uuriti hapniku redutseerumist katalüsaatormaterjalidel, mis põhinesid pürolüüsi teel valmistatud Fe- ja Co-ftalotsüaniiniga (Pc) modifitseeritud šungiidil. Valmistatud materjalide omadusi uuriti mitmete füüsikaliste karakteriseerimismeetoditega. Hapniku elektrokeemilist redutseerumist valmistatud materjalidel uuriti nii aluselises kui ka happelises lahuses. Kõige aktiivsem hapniku redutseerumise katalüsaator aluselise keskkonna jaoks valmistati KOH lahuses töödeldud šungiidist, mis oli modifitseeritud FePc ühendiga. Stabiilsustestid 0,1 M KOH lahuses näitasid valmistatud katalüsaatormaterjalide head stabiilsust. Happelises keskkonnas tehtud eksperimendid näitasid samuti kõige paremat aktiivsust hapniku redutseerumiseks KOH lahuses töödeldud ja FePc ühendiga valmistatud materjalil.
Võtmesõnad: elektrokatalüüs, hapniku redutseerumine, mitte-väärismetallkatalüsaator, šungiit

CERCS: P401 Elektrokeemia

TABLE OF CONTENTS

ABBREVIATIONS

AEMFC Anion exchange membrane fuel cell

CDC Carbide-derived carbon

CNT Carbon nanotubes

CoPc Cobalt(II) phthalocyanine

CV Cyclic voltammetry

EDX Energy-dispersive X-ray spectroscopy

E_p Oxygen reduction peak potential

FePc Iron(II) phthalocyanine

GC Glassy carbon

K-L Koutecky-Levich

LSV Linear sweep voltammetry

OER Oxygen evolution reaction

ORR Oxygen reduction reaction

PEMFC Proton exchange membrane fuel cell

Pc Phthalocyanine

RDE Rotating disc electrode

SCE Saturated calomel electrode

SEM Scanning electron microscopy

XPS X-ray photoelectron spectroscopy

XRD X-ray diffraction

INTRODUCTION

Over the past decades, demand in renewable and environmentally friendly energy sources has increased. Fuel cells and metal-air batteries are the most promising devices for this requirement, due to their high power density and low cost. The oxygen reduction reaction (ORR) is the key process taking place at the cathode of these devices, however due to the slow kinetics, a cathode catalyst has always been required. Many approaches have concentrated on the development of the bifunctional catalysts which could also support the oxygen evolution reaction (OER) since it is an important half-reaction involved in renewable energy technologies, such as metal-air batteries [1].

Up to now, Pt-group metal-based catalysts have been found to be the most active for these reactions. Unfortunately, drawbacks of Pt catalysts have limited the commercialisation of the fuel cells, due to its high cost and limited availability. Many researchers have focused on designing the proper catalysts with the characteristics like high durability, low cost, high surface area and effectiveness and it has been established that carbon-based catalysts as a result of their high surface area could be employed as supports in the ORR catalysis [2].

Shungite is a natural mineral composed mainly of carbon, although its composition varies depending on the mineral deposit. Its energy related applications have not been widely evaluated, however comparison of this material with other carbon-based catalysts has pointed out its superiority over the rest. Therefore, shungite is an attractive novel material for conducting electrochemical studies of ORR and OER [3].

Studies have shown that pristine carbon-based materials are not active enough for this application, therefore their functionalisation with a transition metal like Co or Fe complexes, for example phthalocyanines (Pc) have been reported to significantly enhance the electrocatalytic activity of the material towards the ORR [4].

Therefore, it has been presumed that functionalisation of shungite with FePc and CoPc could lead to a promising ORR and OER catalyst material.

Even though carbon nanomaterials have shown better ORR activity in alkaline conditions than in acidic media, the pH dependence has not yet been elucidated, therefore the ORR studies of shungite modified with FePc and CoPc macrocyclic compounds were conducted in both 0.1 M KOH and 0.5 M H_2SO_4 solutions.

1 LITERATURE REVIEW

1.1 Energy-related application of natural shungite

As it has been studied, the structural peculiarities of carbon in natural shungite, originating from metamorphically complex shungite rocks, have made it the subject for application in various industrial or domestic utilisation [5]. In the past few decades, carbon materials have earned a lot of recognition for their application in the fuel cell catalyst composition, due to beneficial properties [6]. However, there is not enough data gathered about the electrochemical performance of shungite and its derivatives Thus, the key to assessing the opportunities of shungite lies in becoming familiar with its history and composition.

Natural shungite is a black, dark-grey solid mineraloid with a characteristic conchoidal fracture and exists as a mix of several carbon allotropes, in which the crystal lattices are joined by amorphous carbon dated to be formed about 2 billion years ago [7,8]. The term shungite was first brought up by Inostrantsev (1879) for 'a new type of amorphous carbon' from black shales and its first description comes from a deposit near Shunga village, explaining the origin of its name [8,9]. Occurrences of shungite minerals have mostly been reported from Russia, though, several much smaller deposits have been discovered in Kazakhstan and India [10]. The mineral part of shungite rocks is represented, mainly, by Si, Al, Ca, Mg, K, Fe and Ti oxides, which is why pure shungite is infrequently met in nature - usually in a form of a thin, 30 cm wide streaks [11]. Most often, it is present as an impurity in shungite slates and dolomites, that are laid out in Karelia – on the territory of the Zaonezhsky peninsula and around the northern tip of Lake Onega. The industrial values of shungites is most fully determined for Shungskoe and Zazhogino deposits [12,13].

In this study, shungite from Zazhogino mineral deposit was used, in which, shungites are composed of just about 30% carbon and 70% silicates according to the literature [14].

Due to its distinct physical and chemical features, namely, high adsorption capacity, corrosion resistance and catalytic activity, shungite has numerous applications not only in metallurgy but in water purification systems as well. Its low cost, ecological purity, large surface area and harmlessness have contributed for usage of shungite as a filter material or as a sorbent for cleaning contaminated water from pathogenic bacteria and heavy metals [15,16]. Some applications of shungite stones have been encountered in folk medicine since the 18th century [17].

Interest in shungite grew roughly 35 years ago, following the discovery of a new carbon allotrope – buckminsterfullerene. When occurrence of fullerene in natural samples, explicitly, in shungite rocks was first described, industrial attraction was provoked. Although, fullerenes were found only in very low concentrations in shungite minerals (0.1 wt.%) [3].

Energy related prospects of shungite have not been extensively evaluated, however, electrochemical studies, in particular, electrocatalytic behaviour, such as hydrogen evolution reaction (HER) and oxygen evolution reaction (OER), have proven its high potential towards development of a novel natural catalyst material. Catalytic activity of shungite in comparison with other known carbon-based catalyst materials – carbon black, carbon nanotubes (CNTs), fullerene, and glassy carbon has pointed out its superiority by outperforming the rest in the catalytic capability. Reason to such performance lies in the different classes of elements present in the composition of natural shungite [3]. Studying electrocatalytic activity of shungite, most importantly its involvement in fundamental reactions, allows the evaluation of the opportunities of implementing this material in energy conversion and storage devices. Such applications include fuel cells, where these reactions (e.g. oxygen reduction reaction (ORR)) are widely studied in search for the cheaper alternatives to Pt containing catalyst materials for the development of environmentally friendly electrochemical technologies.

1.2 Oxygen reduction reaction

The ORR is the key electrochemical processes occurring at the cathode of the energy conversion and storage devices such as fuel cells or metal-air batteries. The operation principle of the two lies in converting chemical energy into electrical energy via redox reactions, which will be discussed in the following paragraphs.

There are several types of fuel cells and the increasing interest in this field has led to considerable amount of research accumulated over the recent years. General mechanism of fuel cells is the same throughout the types and lies in the following: H_2 (or another fuel, e.g. CH_4) supplied at the anode is oxidised, generating ions and electrons. The ions are channelled through electrolyte towards the cathode, where O_2 is supplied, causing ions and oxygen to react and form water. Necessary electrons to complete this reaction are produced at the anode and are diverted through an external circuit, reaching the O_2 at the cathode and therefore, producing direct current. In order to support the conduction of certain dissolved ions and prevent transport of unwanted species, ion-exchange membranes are employed in the fuel cells. Most noteworthy examples used in fuel cell technologies are the anion exchange membranes (AEM) and proton exchange membranes (PEM). Anion exchange membrane fuel

cells (AEMFCs) use AEM to separate the anodic and cathodic departments. AEM contains positively charged ion-exchange groups, which permit the OH^- anions, generated at the cathode, to migrate towards the anode. Proton exchange membrane fuel cells (PEMFCs) are similar to AEMFC, but the main difference lies in the solid membrane PEM, which creates an acidic environment and supports the transport of H^+ towards the cathode, in the reverse direction of OH^- migration in case of AEMFC [1].

Both, AEMFC and PEMFC have exhibited remarkable performance, however using specific catalyst and conditions, giving rise to difference of opinions about which one of the low-temperature fuel cells is more reliable and efficient in energy conversion. With the intention of evaluating their opportunities, it is important to look at some advantages of one over another.

AEMs have shown significantly lower ionic conductivity than PEMs and need a proper membrane-compatible ionomer. Whereas PEM fuel cells have specifically benefited from the copolymer Nafion®, which has shown excellent proton conductivity and great chemical and thermal stability although, in specific conditions. Usage of Nafion® has strongly improved the overall performance of polymer electrolyte membrane fuel cells. Thus, development of anion exchange membrane with high OH^- conductivity remains a challenge for the researchers. Considering this problem with AEMFCs, studies have succeeded in developing specific appropriate catalyst for AEMFC and PEMFC applications and alterations for achieving better results is still actively taking place [18].

On the other hand, AEMFCs propose quite important advantages over the PEMFC technology. One of which is overcoming the cost barriers of the ORR catalysts: variety of cathode catalysts in alkaline media is much wider, since AEMFCs allow the use of less-expensive and widely accessible, Pt-free catalysts. Operating at high pH supports the ORR kinetics, permitting the use of non-precious metal cathode catalysts prepared using iron and cobalt containing compounds (e.g. phthalocyanines) [1,19–21].

In this context, ORR and OER play a crucial role in Zn-air batteries - a promising energy storage appliances for next-generation electronics. Active cathode catalyst is required to catalyse ORR during discharge. Zn-air batteries are running on the power of oxidization of Zn. OH^- and water are reused at the cathode, without consuming the water. Also, OER catalyst for the cathode is under development for rechargeable batteries. On that account, exploring highly efficient bifunctional catalysts has been the major pursuit to assemble Zn-air batteries [22,23].

Due to high bond energy of the oxygen molecule ($\Delta H° = +498$ kJ mol^{-1}), the ORR is the slowest reaction in any condition of the fuel cells, therefore, to ensure efficient performance, this reaction requires an electrocatalyst that can lower the activation energy barrier in order to get a higher current density from the cathode [2,24]. Up to now, in all fuel cell systems, scarcely available Pt has been considered as a key component in the state-of-the-art electrocatalysts for the hydrogen oxidation reaction (HOR) at the anode and ORR at the cathode. Also, the kinetics of ORR are significantly slower than that of the HOR, leading to a much higher loading of the platinum catalyst at the cathode, than the anode and causing further limitations in the applications of Pt. Due to such high charges and difficulties in obtaining Pt, comprehensive utilisation of fuel cells and batteries has been inhibited [2]. As a result of the sluggish kinetics of the electrochemical ORR, attention of fuel cell research is drawn to the development of the efficient cathode catalyst, however rational design of the material remains a major challenge in the synthesis of the electrocatalysts [1].

The complex multistep ORR process at the cathode proceeds either via 2-electron ($2e^-$) or 4-electron ($4e^-$) reduction pathway, depending on the characteristics of selected electrocatalysts and electrolyte. The two pathways in both alkaline and acidic solutions can be visualised according to the reactions 1) and 2):

1) The direct or $4e^-$ pathway of oxygen reduction to H_2O:

$O_2 + H_2O + 4e^- \rightarrow 4OH^-$ alkaline solution (a)

$O_2 + 4H^+ + 4e^- \rightarrow 2H_2O$ acidic solution (b)

2) The $2e^-$ pathway of oxygen reduction to H_2O_2 followed by reduction of peroxide to H_2O:

alkaline solution: acidic solution:

$O_2 + H_2O + 2e^- \rightarrow HO_2^- + OH^-$ (a) $O_2 + 2H^+ + 2e^- \rightarrow H_2O_2$ (c)

$HO_2^- + H_2O + 2e^- \rightarrow 3OH^-$ (b) $H_2O_2 + 2H^+ + 2e^- \rightarrow 2H_2O$ (d)

In general, electrocatalysts that promote a direct $4e^-$ reduction of O_2 to H_2O are preferred over those involved in the $2e^-$ reduction process, so, in order to gain maximum energy from the reaction, the two step $2e^-$ reduction pathway and hydrogen peroxide formation should be avoided, since not only it causes the degradation of the fuel cell parts, but also leads to lowering of working current and potential efficiencies [1,25]. For comparison of oxygen reduction reaction pathways between various electrocatalysts Table 1 can be addressed.

Table 1. Comparison of ORR pathways throughout several electrocatalyst materials.

4e⁻ reduction	**2e⁻ reduction**
Pt	Glassy Carbon
Carbon supported Pt catalyst (Pt/C)	Graphene
Iron phthalocyanine (FePc) [26]	Carbon Materials Catalysts (CMC) [27]
Ru [28]	Pristine CNTs [29]

Considerable amount of studies have been conducted to try to reduce the cost of catalysts and the efforts are still in the research state, as their activity and stability are generally still lower than that of the Pt-based catalysts.

1.2.1 Transition metal macrocycles for ORR

Transition metal macrocycles (TMMs), containing porphyrin or phthalocyanine ligands have been studied as ORR catalysts since the 1960s and up to now, cobalt and iron phthalocyanines (CoPc and FePc, respectively) remain the most-studied macrocyclic compounds for the fuel cell cathode catalyst application [30].

Phthalocyanine (Pc) is a planar, aromatic macrocycle built up of four iminoisoindole units, able to host ions from over 70 elements. From the structure of phthalocyanine (Figure 1) it can be seen that the chelating group which coordinates the central metal ion for the TMM complex formation is the four nitrogen atoms (N_4) [31]. The first finding of transition metal phthalocyanine (TMPc) as ORR electrocatalysts has stimulated the research for development of such materials for further applications.

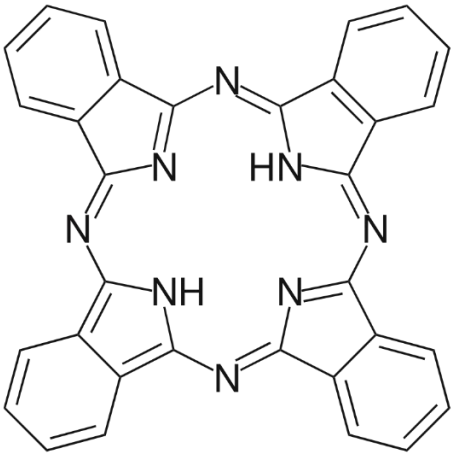

Figure 1. Structural formula of phthalocyanine [32].

In this regard, MN_4 macrocyclic complexes - metal phthalocyanines, have been explored as non-precious model systems; different heat-treatment protocols have been exploited to synthesise the best high-performance catalysts and large sets of ORR data have been collected [33]. Studies have shown that poor electric conductivity of macrocyclic compounds has affected the electron transport in the catalytic process, resulting in low limiting-current densities. Due to their characteristics, such as high surface area, high porosity and excellent electron conductivity, carbon materials have been considered as novel catalyst supports in the electrocatalytic processes. Numerous efforts have been made to develop non-precious metal catalysts, such as metal-N_4 macrocycles, pyrolyzed transition metal/nitrogen-containing complexes supported on various carbon materials and doped carbon nanomaterial with heteroatoms [2,34–36].

FePc catalyst are the largest class of TMPc catalysts, which have been explored due to their higher or comparable electrocatalytic ORR activity to Pt/C. In general, FePc-based catalysts can demonstrate the ability to directly promote $4e^-$ ORR with H_2O as a final product. To improve the catalytic ORR activity of FePc materials, several research groups have decided to support FePc catalysts on a variety of high surface area carbon materials. Pcs adsorb strongly on carbon nanomaterials through noncovalent π–π interactions. Recently, carbon nanotube-supported FePc and CoPc complexes have been employed as electrocatalysts for cathodic oxygen reduction and such functionalisation was reported to enhance the electrocatalytic features of these complexes [4].

It has been established that the properties of support material to which the TMPc is attached to, also has an important influence on the electrocatalytic activity. Few years ago, graphene and graphene-based materials have been studied as novel catalyst supports for FePc-based catalysts. For example, catalyst materials prepared by functionalisation of graphene oxide nanosheets with iron(II) phthalocyanine have shown excellent electrocatalytic activity towards the ORR in alkaline media [34,37].

In the number of catalyst supporting carbon materials, carbide-derived carbon (CDC), has caught attention as electrocatalyst support material due to its properties, such as large specific surface area, porosity, electrical conductivity and corrosion resistance. Recently, Praats et al. showed that electrochemical behaviour of FePc functionalised CDC catalysts exhibit similar or higher ORR electrocatalytic activity than that of Pt/C catalyst [38].

Activities of composite catalysts, such as FePc modified reduced graphene oxide/multi-walled carbon nanotube (rGO/MWCNT) have been also investigated. CNT-based catalysts

in fuel cells have attracted a great deal of attention due to their excellent properties like high electrical conductivity, large surface-to-volume ratio and corrosion resistance. The results show that FePc modified rGO/MWCNT electrocatalysts heat-treated at 800 °C are highly active for ORR in alkaline solution [39]. In addition, the electrocatalytic performance of pyrolysed FePc modified CDC/CNT composite materials have also shown outstanding AEMFC performance [40].

The second largest type of TMPc-based catalysts for ORR is CoPc-related materials. CoPc-based electrocatalyst have been reported to have the capability to follow the $4e^-$ ORR pathway to water without the formation of peroxide intermediates, even though most CoPc-based materials are prone to exhibit $2e^-$ oxygen reduction. In the literature, various carbon materials have been explored as catalyst supports, such as carbon blacks, mesoporous carbons, pyrolytic graphite, CNTs and graphene-related materials [34,39].

The studies of the above-mentioned rGO/MWCNT catalyst material includes functionalisation of the composite with Co(II) phthalocyanine, showing a noteworthy performance in alkaline media, however, the superior performance was observed in case of Fe(II) phthalocyanine-based catalyst in the same work [39]. As an example of CoPc-modified composite material activity, a recent study of O_2 electroreduction on CoPc-functionalised CDC and CNT composite catalysts can be addressed. Catalysts with various CDC to CNT ratios were studied, resulting in the higher ORR electrocatalytic activity of composites with higher CNT content. Such materials also possessed remarkable AEMFC performance [41].

Some researchers have concentrated on TMM-modified nanofiber catalysts, by comparing electrochemical activities of different Co and Fe-containing catalysts in acidic medium. Electrochemical studies have revealed that pyrolysed Fe-based catalysts show higher ORR activity than their Co counterparts. Moreover, Fe-containing catalysts were reported to promote the $4e^-$ reduction, whereas Co ones followed the $2e^-$ pathway with the production of H_2O_2 [42].

Another work, which studied the mechanisms of the ORR on FePc/C and CoPc/C in alkaline solution showed that CoPc/C catalyst follows the $2e^-$ reduction pathway, however under the fuel cell cathode conditions FePc was much less stable than CoPc in this specific study [43].

As it has been found, the type of the central metal atom influences the catalytic activity, and despite the huge effort in developing MN_4 macrocycles as fuel cell electrocatalysts, these compounds have not demonstrated both an acceptable ORR catalytic activity and stability as compared to Pt-based catalysts. Nevertheless, this vast amount of research is providing

useful data not only for the rational design of highly active non-precious metal catalyst for ORR, but also about the enhancement of the durability of implemented electrocatalysts [33].

There is still a lot of research needed to be conducted for designing and developing an appropriate cathode catalyst, therefore it is important to study the materials which provide high reliability as a result of their composition. From this perspective, shungite has not been examined enough, and due to its specific physical and chemical properties, is introduced as a bifunctional catalyst. As reported, shungite has surpassed the catalytic activities of other carbon-based and metal loaded carbon materials such as CNTs, fullerene and GC [3].

Interestingly, composition of shungite materials is similar to the previously studied silicon oxycarbide (SiOC), which possesses high chemical, thermal stability and semiconducting behaviour due to amorphous structure originating from SiO_2/C nanodomains. Furthermore, the SiOC based materials showed high ORR activity after codoping with N and Co. Such results of SiOC-based electrocatalysts show that this material can be considered in future development as ORR catalysts for fuel cell technology. Similarly, energy-related applications of shungite show that its complex structure contributes to its performance, therefore, functionalisation of this compelling material with the high-performing and promising TMMs could lead to a novel cathode ORR catalyst material of a natural origin [3,44].

2 THE AIMS OF THE THESIS

Main objectives of the present research lie in the following:

- Investigate electrocatalytic oxygen reduction reaction activity of Iron(II) phthalocyanine and Cobalt(II) phthalocyanine functionalised natural shungite material.
- Study the electrochemical activity of shungite in alkaline and acidic environments.
- Analyse the surface and elemental composition of the prepared shungite-based electrocatalyst.
- Develop a novel oxygen reduction reaction catalyst material.

3 EXPERIMENTAL

The results of present bachelor's thesis are divided into two main parts as physical and electrochemical characterisation. Physical characterisation experiments were conducted by the following researchers: SEM-EDX analysis – Dr. Jekaterina Kozlova, XPS analysis – Dr. Arvo Kikas; Raman spectroscopy – Dr. Alexey Treshchalov and XRD analysis – Dr. Jaan Aruväli. Description of the physical characterisation data and all the electrochemical experiments with corresponding analysis were done by the author of this bachelor's thesis.

3.1 Preparation of catalyst materials

Initially, natural shungite material (TY 5714-007-12862296-01, cut and granulated shungite of Zazhoginskoye mineral deposit, Republic of Karelia, Russian Federation) was ground with ZrO_2 balls (5 mm in diameter) using a dry-milling procedure as follows: 500 rpm for 5×30 min with 5 min breaks for cooling. This material is referred to as SHUa. Afterwards, SHUa was treated with 25% KOH (p.a. quality, Merck) solution, according to the literature [45]. In a typical experiment, 3g of SHUa, 28 mL of Milli-Q water (Millipore, Inc.), 12 g of 85% KOH pellets were mixed and stirred using an ultrasonic bath. After 2 h of sonication, the suspension was filtered with polyethersulfone (PES) membrane (pore size = 0.2 μm) and then dried in vacuum at 60 °C, 20 mbar. This material is designated as SHUb in this work.

In addition to 25% KOH treatment, SHUb was leached in HF and HNO_3 mixture, yielding the material named SHUc. This procedure was compiled according to the literature [46]. Leaching took place in a Teflon® beaker with a magnetic stirrer (250 rpm) containing 1.2 g of SHUb, 29 g of 40% HF (Merck), 30 mL of 65% HNO_3 (Merck) and 10 mg of $NaNO_2$ (Merck). After 2 and 5 h from the start of this 12 h procedure, additional 30 mg of $NaNO_2$ was added into the solution. After leaching, the material was washed and filtered three times with 0.5 M HNO_3 and with Milli-Q water, followed by drying overnight at 60 °C.

The functionalisation of shungite with transition metal macrocyclic complexes was carried out in accordance with the previously published modification procedure [40]. The solution was prepared by dispersing iron(II) phthalocyanine (FePc, Acros Organics) or cobalt(II) phthalocyanine (CoPc, Alfa Aesar) and equal amount of SHUb or SHUc in 25 mL of 2-propanol (99.8%, Honeywell Riedel-de Haën). The solution was placed in the ultrasonication bath for 2 h and later dried overnight at 60 °C. The obtained mixture was transferred to a ceramic boat and pyrolysed in a quartz tube furnace (MTF 12/38/400, Carbolite) in the flowing N_2 environment. The furnace was heated up to 800 °C using a heating rate of 10 °C

min^{-1} and kept at that temperature for 2 h. After pyrolysis, the furnace was slowly cooled down to room temperature. The resulting materials bear additional designation of Fe/N or Co/N corresponding to the modification of shungite with FePc of CoPc, respectively.

Further acid leaching was performed with several materials according to the previously published procedure [47]. In particular, the material was treated with 25 mL of 0.5 M H_2SO_4 + 0.5 M HNO_3 acid mixture and stirred with a magnetic stirrer at 1100 rpm, at 50 °C for 8 h. The obtained material was filtered and pyrolysed for the second time, similarly to the above-mentioned carbonisation procedure. These materials are additionally marked with -A in their designations.

3.2 Electrode preparation

Glassy carbon (GC) electrodes with a surface area of 0.196 cm^2 were used as a substrate for depositing catalyst materials. The GC discs (GC-20SS, Tokai Carbon, Japan) were fixed into Teflon® holders and were polished using 1 and 0.3 μm alumina slurry (Buehler), followed by removal of polishing debris by sonicating the electrodes in Milli-Q water and 2-propanol for 5 min in each solvent. Catalyst ink for electrochemical measurement in 0.1 M KOH was prepared using 8 mg of catalyst material, 2 mL of 2-propanol and 10 μL of Nafion® (5 wt%, Aldrich) as an ionomer. As for the measurements in 0.5 M H_2SO_4, 12 mg of SHU, 1.5 mL of 2-propanol and 15 μL of 5% Nafion® was used. In both cases, suspensions were sonicated for 90 min. For testing in 0.1 M KOH, 10 μL of the catalyst ink was pipetted onto the GC surface, resulting in 0.2 mg cm^{-2} loading. For experiments in 0.5 M H_2SO_4, 20 μL of catalyst ink was drop cast onto the electrode, giving a catalyst loading of 0.8 mg cm^{-2}. The solvent from the catalyst suspensions was let to evaporate in air.

3.3 Surface morphology and composition studies

Surface morphology of shungite-based electrocatalysts was examined using scanning electron microscopy (SEM). SEM samples were prepared by dispersing 8 mg of catalyst into 2 mL of 2-propanol. The suspension was drop cast onto the GC discs. For SEM experiments, high-resolution scanning electron microscope (HR-SEM) Helios NanoLab 600 (FEI Company) equipped with an energy-dispersive X-ray (EDX) spectrometer analyser INCA Energy 350 (Oxford Instruments) was employed. EDX spectroscopy was used to identify the elemental composition and distribution in catalyst materials.

X-ray photoelectron spectroscopy (XPS) was also employed for physical characterisation of the catalysts, where GC plates (11 × 11 mm^2) were coated using the same catalyst ink as for

the preparation of the SEM samples (without Nafion®). The XPS samples were analysed with SCIENTA SES-100 spectrometer with a 300-W non-monochromatic Mg Kα X-ray source (incident energy = 1253.6 eV) and Al Kα (1486.6 eV) were used for SHUb-Co/N-A and SHUb-Fe/N-A, respectively, with the electron take-off angle 90º. The pressure inside the analysis chamber was below 10^{-9} Torr during the XPS spectra collection. The step size of 0.5 and 0.1 eV was used for collecting survey spectra and core-level XPS spectra; with pass energy of 200 eV.

The catalysts were also studied using Micro-Raman spectroscopy. Raman spectroscopy measurements in backscatter geometry were done using a Renishaw inVia spectrometer with a confocal microscope and the excitation wavelength from the Ar ion laser of 514.5 nm. The laser power on the sample was below 3 mW. Samples were prepared using the same catalyst ink as for SEM investigation and dropped onto Si-wafer.

X-ray diffraction (XRD) analysis was used to study the phase composition of shungite. Analyses were performed using Bruker D8 Advance diffractometer with Ni-filtered Cu Kα radiation. The XRD patterns were collected with a counting time of 525 s per step, with a step of 0.013°2θ from 5 to 85°2θ.

3.4 Electrochemical studies

Three-electrode system was used for electrochemical measurements, where GC electrode coated with catalyst ink served as the working electrode, Pt wire as a counter electrode and saturated calomel electrode (SCE) was used as reference electrode (all potential values in this Bachelor thesis are given with respect to SCE). Experiments were carried out in Ar-saturated (99.999%, Linde) or O_2-saturated (99.999%, Linde) aqueous electrolyte solutions of 0.1 M KOH or 0.5 M H_2SO_4 (Suprapur, Merck). Potential to the working electrode was applied with an Autolab potentiostat/galvanostat PGSTAT30 (Metrohm Autolab). Cyclic voltammetry (CV), linear sweep voltammetry (LSV) and rotating disc electrode (RDE) methods were employed for the electrochemical experiments, which were controlled by Nova 2.1 software. The RDE measurements were performed at different rotation rates (ω) ranging from 360 to 4600 rpm using EDI101 rotator and a CTV101 speed control unit and the polarisation curves for ORR experiments were recorded in cathodic direction. In addition, the oxygen evolution reaction (OER) was studied on different catalyst materials in Ar-saturated 0.1 M KOH solution and the OER polarisation curves were recorded in the anodic direction.

4 RESULTS AND DISCUSSION

4.1 Physical characterisation

Scanning electron micrographs presented in Figures 2 and 3 depict the surfaces of SHUa, SHUb, SHUb-A and SHUc materials at two different magnifications. From the topography of SHUa in Figure 2a it can be seen that grinding the initial natural shungite material with ball milling at 500 rpm has resulted in a fine powder, containing particles ranging from several hundreds of nanometres to approximately 5 micrometres in size. In case of SHUb, shown in Figure 2b, somewhat larger particles are observed as a result of 25% KOH treatment followed by filtration with PES membrane filter (pore size 0.2 μm).

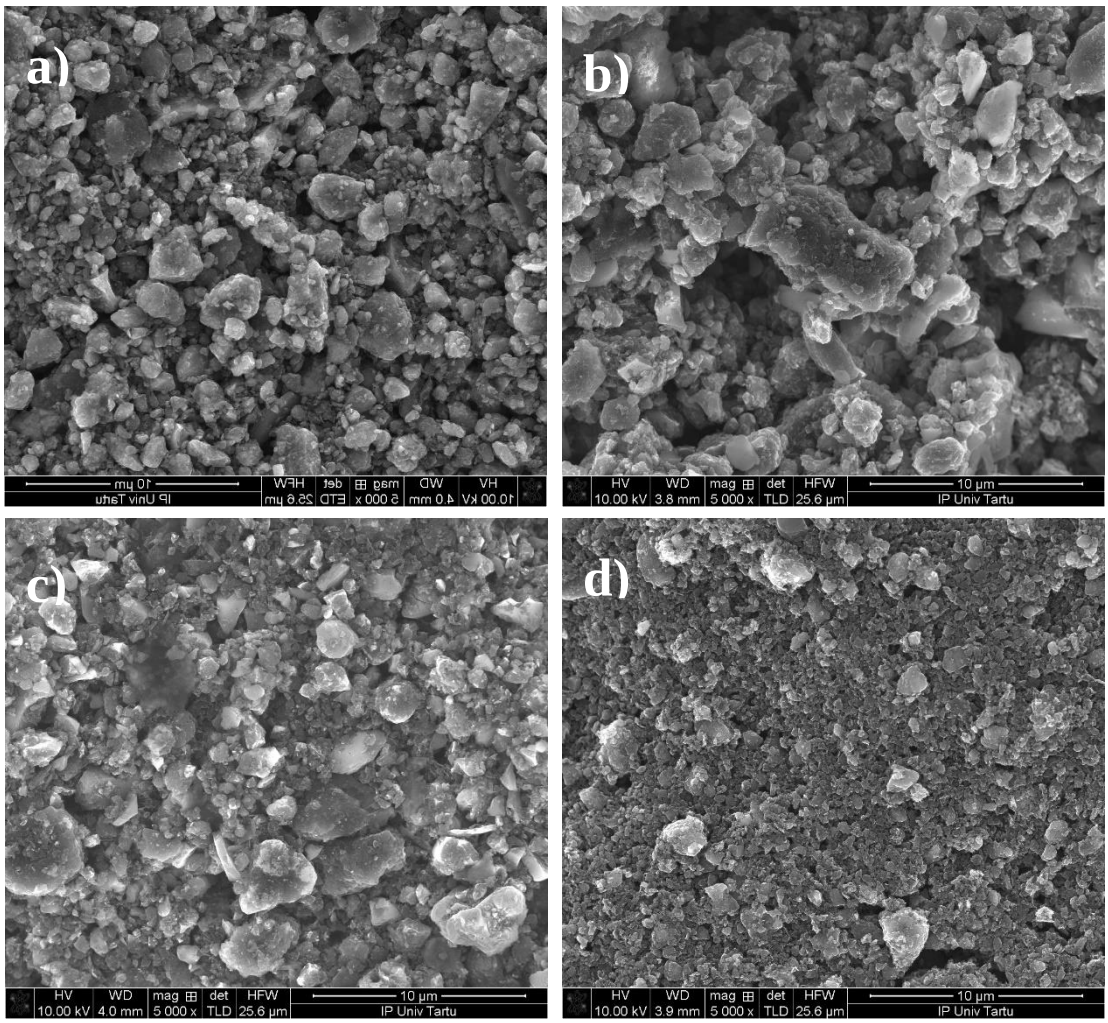

Figure 2. SEM micrographs of a) SHUa, b) SHUb, c) SHUb-A and d) SHUc samples (5000× magnification, scale bar: 10 μm).

Regarding the acid treatment, there is no significant visible change in the structure of SHUb-A material in Figure 2c. Particle sizes of unmodified ball-milled shungite as compared to

other studies of shungite, is quite the same and the grains remain less or no more than 10 μm [11,48].

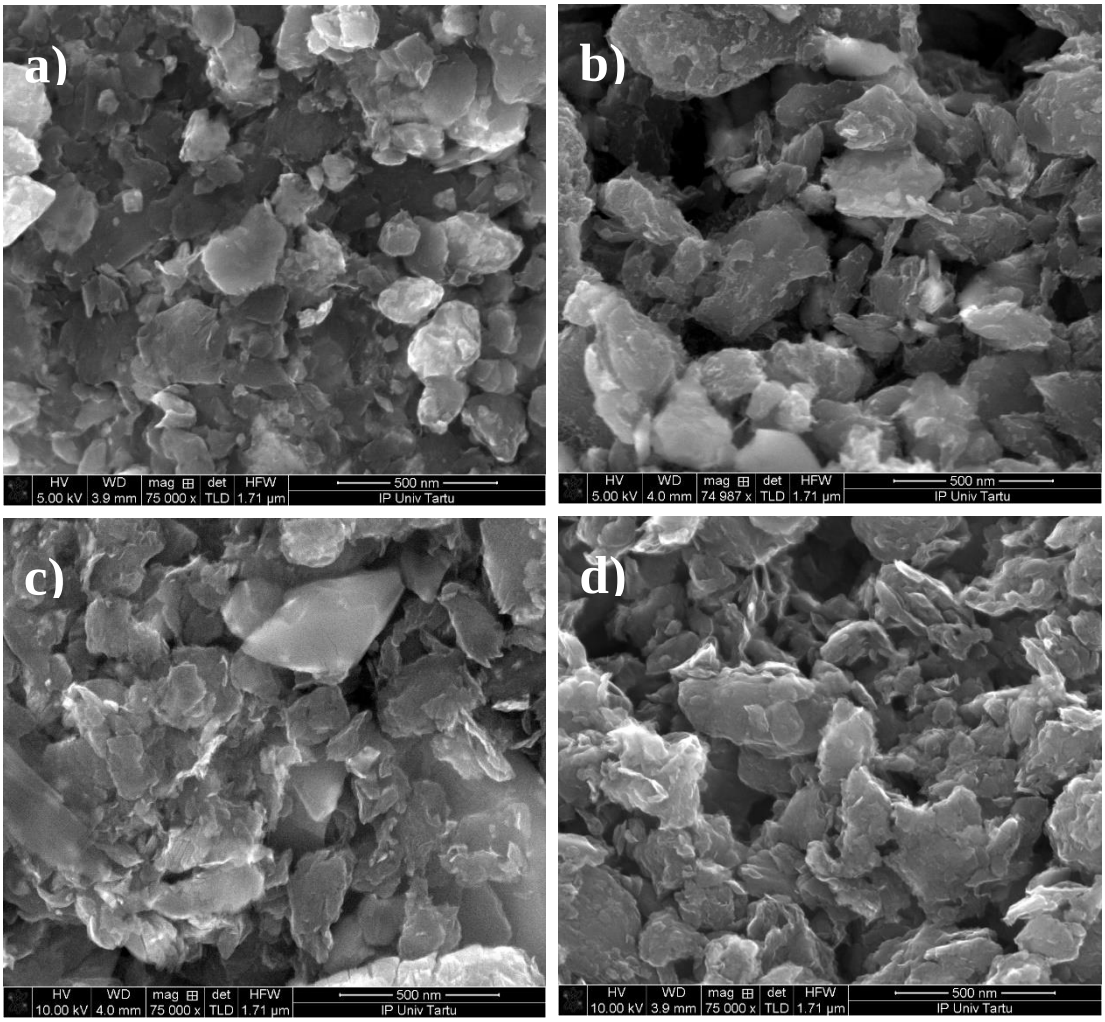

Figure 3. SEM micrographs of a) SHUa, b) SHUb, c) SHUb-A and d) SHUc (75 000× magnification, scale bar: 500 nm).

Elemental composition of natural shungite not only varies among different mineral deposits, but also, evidently, shungite minerals obtained from the same deposit can contain distinct components. According to previously studied shungite of Shunga village, the EDX studies revealed that the raw material contained 90.2 wt.% of C and traces of O, Fe and Al [49]. As stated in the preceding study, shungite from Zazhogino deposit was reported to consist of 30% carbon and 70% silicates. Expectedly, the EDX studies of shungite of Zazhogino deposit used in this study revealed dissimilar composition as shown in Table 2. Although, another research, which performed EDX elemental analysis of shungite from this deposit showed that C and SiO_2 content were 31.3% and 42.7%, respectively [11].

Results of the EDX analyses presented in Table 2 indicate that the ball-milled natural material SHUa contains ca. 30% wt of C and the rest of the weight is mainly comprised by Si, Al, Fe, Ti, in an oxide form or in the composition of salts; this composition does not significantly vary among SHUa and SHUb materials. It is worth mentioning, that after acid leaching, there has been an elimination of the Fe (0% wt.) and reduction in Mg (0.2% wt.) content. As it can be seen from Figure 2d, SHUc appears in comparatively smaller particles most likely due to the particle degradation by Si removal during HF/HNO_3 leaching, with only a few particles with size $\geq 5\mu m$.

Table 2. Elemental composition as determined by EDX analysis of non-modified SHUa, SHUb, SHUb-A and SHUc materials (wt%).

Catalyst material	**C**	**N**	**O**	**F**	**Mg**	**Al**	**Si**	**S**	**K**	**Ti**	**Fe**	**Co**
SHUa	27.4	0.0	37.6	0.0	0.4	2.2	26.2	1.8	1.1	0.2	3.2	0.0
SHUb	32.9	0.0	35.2	0.0	0.4	1.5	25.7	0.3	0.9	0.2	3.1	0.0
SHUb-A	36.1	0.0	36.2	0.0	0.2	1.6	25.0	0.1	0.7	0.2	0.0	0.0
SHUc	89.0	2.8	7.3	0.3	0.0	0.0	0.0	0.5	0.0	0.1	0.0	0.0

Since SiO_2 has not been recognised to enhance the ORR activity, it was intended to remove Si from SHUb material by leaching it in HF/HNO_3 mixture based on the procedure taken from the literature [46]. Etching shungite in such harsh conditions has caused the introduction of new elements into the composition, such as F (0.3% wt.) and N (2.8% wt.). According to the EDX results, the removal of Si and its oxide has been successful and this treatment has resulted in a material containing 89% wt. of C. This procedure accounts for removal of Fe, Mg, Al and K, also decrease in Ti residue. The removal of Si could be supported by the SEM images, where larger particles, which most likely were held together with SiO_2, could have split into smaller ones after etching. By comparing SEM images in Figure 3, it can be assumed that on this scale, sizes of the particles remain quite the same among the materials and in case of SHUc the building block of these pieces is primarily carbon.

XRD analysis method was used for identification of crystal phases of the electrocatalysts. The XRD results are presented in Table 3, for XRD spectra supplementary material can be

addressed (see Figures S1-S7). All the materials show similar peaks in the diffraction pattern, which correspond to carbon in the form of graphite 2H and quartz, although, as expected, the latter is not present in case of SHUc material, and additional graphite 3R peaks are observed as a result of the aforementioned HF/HNO_3 leaching. Graphite structures, 2H and 3R have different arrangements of the hexagonal graphene layers [50]. In addition to carbon and quartz content, composition of raw ball-milled shungite is presented by muscovite, pyrite and jarosite minerals, indicating the presence of metallic species such as Fe, Al, K, Mg and Ti in the natural material.

Modification of SHUb with FePc has resulted in peaks of metallic Fe, magnetite and iron carbide. After acid treatment – in SHUb-Fe/N-A, there are peaks referring to Fe most likely only from the FePc functionalisation. Interestingly, in case of CoPc modified SHUb, other than metallic cobalt, iron was also registered in the form of CoFe alloy, since iron was already incorporated in the natural composition of shungite and as presumed, was eliminated due to the acid treating as seen in SHUb-Co/N-A material. Expectedly, metallic species such as Fe, Al and K were no longer present in the SHUc material, the only detected peaks corresponding to metal content was for TiO_2 (anatase), as Ti was also present in the initial ball-milled material.

In the previously mentioned study of shungite from Zazhogino deposit,the XRD analysis has also been conducted, where presence of SiO_2, Fe_2O_3, C and Al_2O_3 was identified. Although, the content of SiO_2 was reported to be higher than in the material used in the present study. In addition, composition included Na_2O and $CaCO_3$, which, according to the XRD analysis, have not been identified for the shungite used herein [48]. Such differences underline that composition of shungites, as natural minerals, is specific to each shungite material obtained through mining.

Raman spectroscopy was employed for further characterisation of the catalyst materials. Raman spectra for the samples are presented in Figure 4. Typical peaks for carbon materials, referred to as the G peak (graphitic) at ~ 1590 cm^{-1} and at ~ 1380 cm^{-1}, ~ 1130 cm^{-1} known as the disordered peaks (D, D*) are observed in all materials. The HF/HNO_3 treated SHUc material exhibits additional defects at ~1134 cm^{-1} and at 1525 cm^{-1}. Such peaks are infrequently met in literature; however, some studies suggest that band at approximately ~ 1188 cm^{-1} can be assigned to sp^2-sp^3 bonds from C-C and C=C stretching vibrations of polyene-like chains. As for the ~ 1525 cm^{-1}, according to Cuesta et al. is related to the occurrence of organic molecules, forming "amorphous" carbon phase [51,52].

Table 3. XRD results for the catalyst materials. The presented values correspond to the wt% of the component and the average crystallite size (nm) is given in the brackets.

Catalyst Material	**SHUa**	**SHUb**	**SHUc**	**SHUb-Fe/N**	**SHUb-Fe/N-A**	**SHUb-Co/N**	**SHUb-Co/N-A**
Graphite 2H	61.34 (1.8)	51.07 (2.8)	48.79 (1.7)	67.51 (2.4)	67.79 (2.4)	73.19 (2)	74.33 (2.1)
Quartz	30.06 (137.1)	38.36 (184.1)		22.62 (161.8)	28.10 (154)	19.40 (167.4)	20.63 (184)
Muscovite	6.39 (27.6)	10.01 (27.2)	–	–	–	–	–
Pyrite	0.3 (86.1)	0.56 (36.4)	–	–	–	–	–
Jarosite	1.91 (52.1)	–	–	–	–	–	–
Fe	–	–	–	0.36 (72.7)	–	–	–
Fe_3O_4	–	–	–	0.95 (16.6)	1.30 (34.2)	–	–
Fe_3C	–	–	–	3.64 (26)	–	–	–
Potassium mica dehy-droxylated	–	–	–	4.92 (40)	2.81 (27.3)	4.82 (24.3)	4.47 (15)
Co	–	–	–	–	–	1.99 (22.4)	0.57 (18.9)
CoFe	–	–	–	–	–	0.60 (14.8)	–
Graphite 3R	–	–	51.07 (3.5)	–	–	–	–
Anatase	–	–	0.14 (40)	–	–	–	–

The Raman spectroscopy study conducted with shungite materials have reported peaks at similar frequencies when compared to shungite in this study. The observed signals are associated with the G-band (at 1582 cm^{-1}), D-band from the optical phonon and the D* for the unconfirmed sp^2-sp^3 bonds [53].

The I_D/I_G ratios were calculated to be 1.8-1.9 for SHUb and SHUc materials as their spectra are largely similar, although the HF/HNO_3 treatment added new defects at 1134 and 1525 cm^{-1} into the SHUc material. Higher I_D/I_G ratios were observed for the functionalised materials resulting in 2.0, 2.1, 2.5 and 2.5 corresponding to SHUb-Fe/N, SHUb-Fe/N-A, SHUb-Co/N and SHUb-Co/N-A samples, respectively, indicating the defective structure as a result of covalent functionalisation of the shungite material with MN_4 metallic centres from FePc and CoPc macrocyclic compounds.

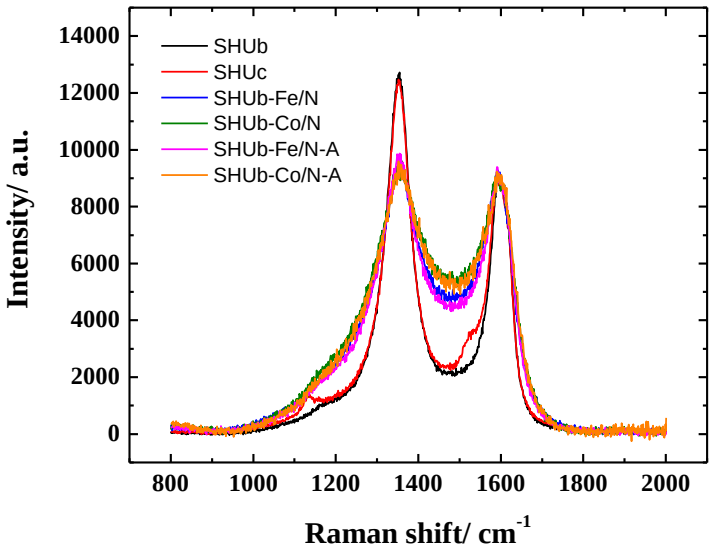

Figure 4. Raman spectra for SHUb, SHUc, SHUb-Fe/N, SHUb-Fe/N-A, SHUb-Co/N and SHUb-Co/N-A materials.

EDX analysis provided with the bulk composition of the materials and since the ORR takes place on the surface of the material, surface composition of the two electrochemically most active catalysts was further evaluated using the X-ray photoelectron spectroscopy (XPS) method. Figures 4 and 5 present the XPS spectra for SHUb-Fe/N-A and SHUb-Co/N-A materials, respectively. Elemental composition obtained from the XPS data is given in Table 4.

Table 4. Elemental composition (at%) of SHUb-Fe/N-A and SHUb-Co/N-A materials as etermined from the XPS; and relative content (%) of various nitrogen species: N1 – pyridinic-N, N2 – metal-Nx, N3 – pyrrolic-N, N4 – graphitic-N, N5 – bulk N-H, N6 – pyridine-N-oxide.

	C	**O**	**Si**	**N**	**Fe**	**Co**	**N1**	**N2**	**N3**	**N4**	**N5**	**N6**
SHUb-Fe/N-A	80.59	12.32	3.08	3.24	0.76	–	34	9	25	24	7	1
SHUb-Co/N-A	76.12	14.26	3.5	5.29	–	0.74	34	13	27	19	5	2

Figures 5a and 6a depict the survey spectra of SHUb-Fe/N-A and SHUb-Co/N-A materials, respectively. Both spectra contain peaks of Si, C, N, O and corresponding transition metals (Fe or Co), as expected. Observed Si peak near 103.5 eV represents the Si2p photoelectrons, indicating the presence of SiO_2 in the material [54]. O1s correspond to the oxygen in the SiO_2, although the amount is higher than what is required for SiO_2 and as the analysis showed, O1s also belong to the transition metal oxides and carbon-oxygen bonds of carboxyl and carbonyl group presented in the composition of the catalyst.

Figures 5b and 6b present the deconvoluted high-resolution XPS spectra in the C1s region for the corresponding catalysts. C1s peaks mainly conform to the sp^2 carbon making up ca. 60-70 at% of the surface composition in case of both catalyst materials. Interestingly, the deconvolution of C1s spectra provided the sp^3 carbon peak only for SHUb-Co/N-A material. N1s peaks for both materials are presented by different N species. N1s XPS spectra can be viewed in Figures 5c and 6c (see also Table 4 for relative content of N species), in which the peak near 398 eV is assigned to pyridinic-N. The presence of pyridinic-N in the electrocatalyst is considered as one of the reasons for high ORR activity, as they catalyse the reduction of O_2 via $4e^-$ pathway, which is beneficial for the ORR process. N1s spectra are also presented by metal-Nx species with peak near 401 eV, referring to the successful functionalisation with FePc and CoPc macrocyclic compounds, which is also considered highly beneficial for the ORR. Similar N1s peak composition to SHUb-Fe/N-A and SHUb-Co/N-A materials have been observed in FePc and CoPc modified reduced graphene oxide and multi-walled

CNT (rGO/MWCNT) composite catalysts, which are appealing ORR catalysts for application in AEMFC [39,55] .

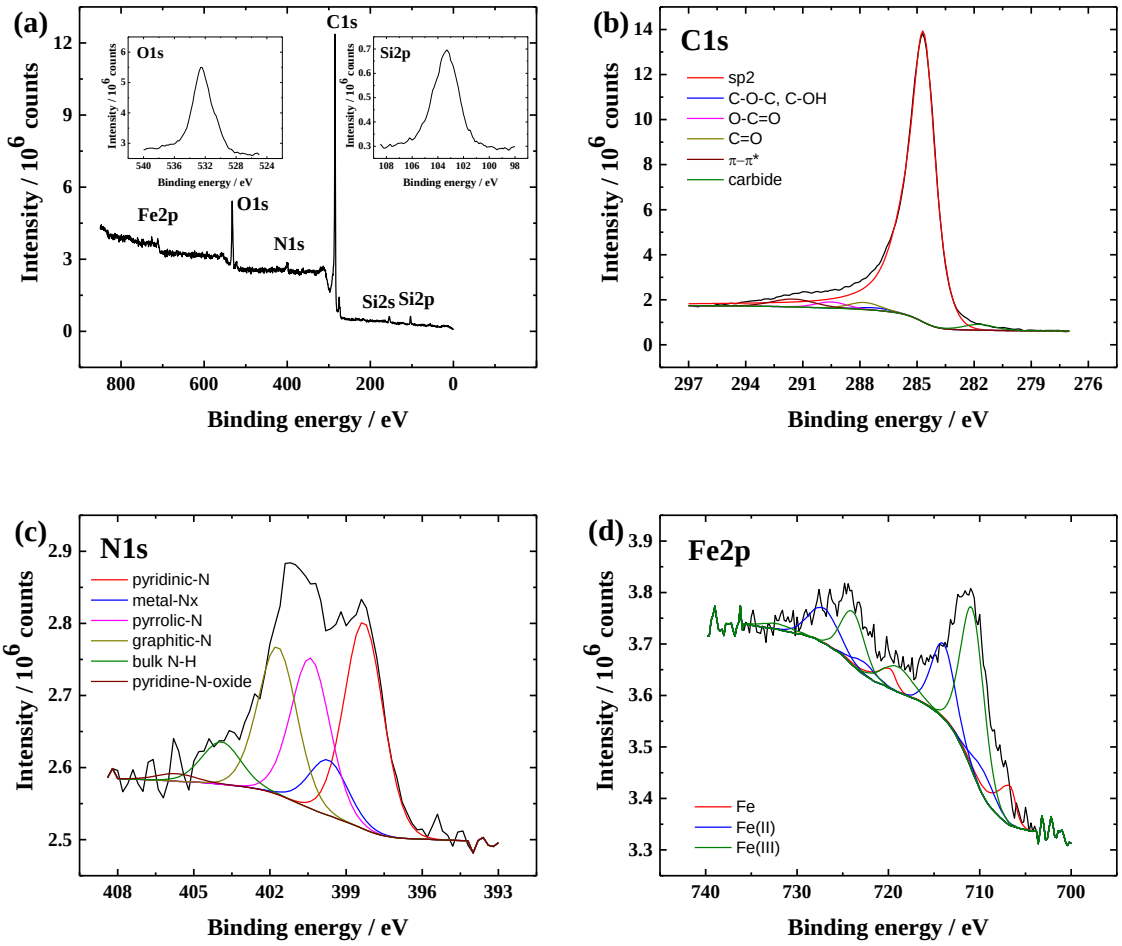

Figure 5. XPS studies with SHUb-Fe/N-A material: (a) survey spectrum with the insets for high-resolution spectra in O1 and Si2p regions. High-resolution XPS spectra in (b) C1s, (c) N1s, and (d) Fe2p regions.

Figures 5d and 6d correspond to the deconvoluted Fe2p and Co2p high-resolution spectra, respectively. In the XPS spectra of Fe2p and Co2p, photoelectrons of transition metals in the metallic state as well in different oxidation states were detected. In Figure 5d, the peak near 709 eV originates from the $Fe2p_{3/2}$ emission, similarly observed in the FePc modified rGO materials, as well as in the CDC/CNT/FePc catalysts [38]. In the Co2p spectra (Figure 6d), peak near 780 eV represents Co2p emission, observed likewise in the CoPc functionalised CDC/CNT composite catalyst [41]. It has been studied, that the acid treatment lowers the metallic content – as observed in the EDX results of SHUb-A, where Fe content was no longer detected (see Table 2). However, the presence of Fe2p and Co2p peaks in the XPS

spectra of SHUb-Fe/N-A and SHUb-Co/N-A materials after acid treatment are the evidence for the successful functionalisation of shungite with the FePc and CoPc complexes [41].

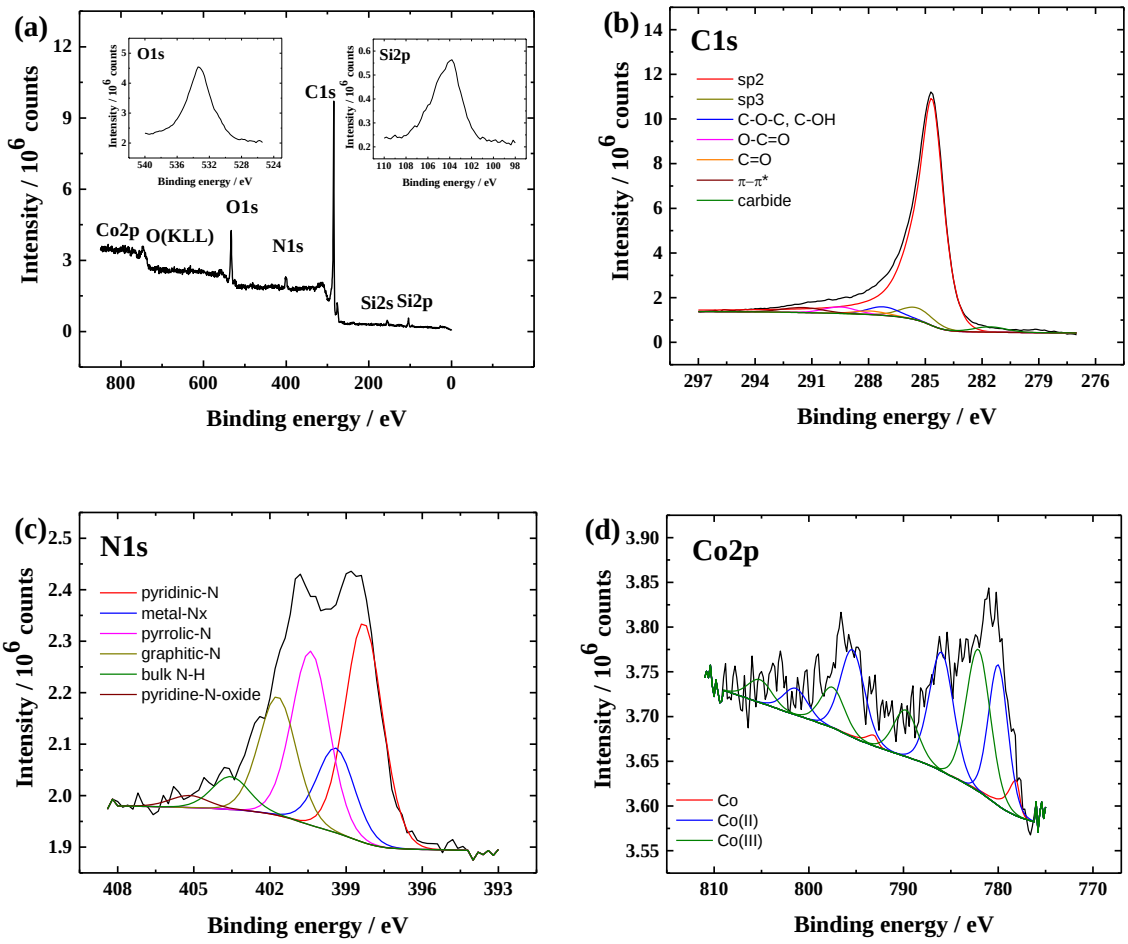

Figure 6. XPS studies with SHUb-Co/N-A material: (a) survey spectrum with the insets for high-resolution spectra in O1 and Si2p region. High-resolution XPS spectra in (b) C1s, (c) N1s, and (d) Co2p regions.

4.2 Electrochemical characterisation

4.2.1 ORR studies in 0.1 M KOH solution

Cyclic voltammograms (CVs) in Ar-saturated 0.1 M KOH solution recorded for unmodified SHUa, SHUb, SHUb-A and SHUc materials deposited onto GC electrodes in comparison with bare GC are presented in Figure 7a. As can be seen, a decrease in capacitive current, originating from small electroactive surface area and decrease in double layer capacitance is observed for the SHUb-A material. A pair of redox peaks corresponds to the oxidation and reduction of Fe species in SHUa and SHUb materials as corresponding peaks have been

registered at very similar potential values during CV experiments in 0.2 M NaOH with Fe cuboid nanoparticles supported on GC and bulk Fe electrodes [56]. The Fe oxidation peak is observed in the anodic scan near -0.69 V vs SCE for both materials. In the cathodic process, peak close to -1.07 V vs SCE corresponds to Fe reduction. As physical characterisation of these materials has shown, SHUc and SHUb-A are Fe-free, therefore such peaks are not observed.

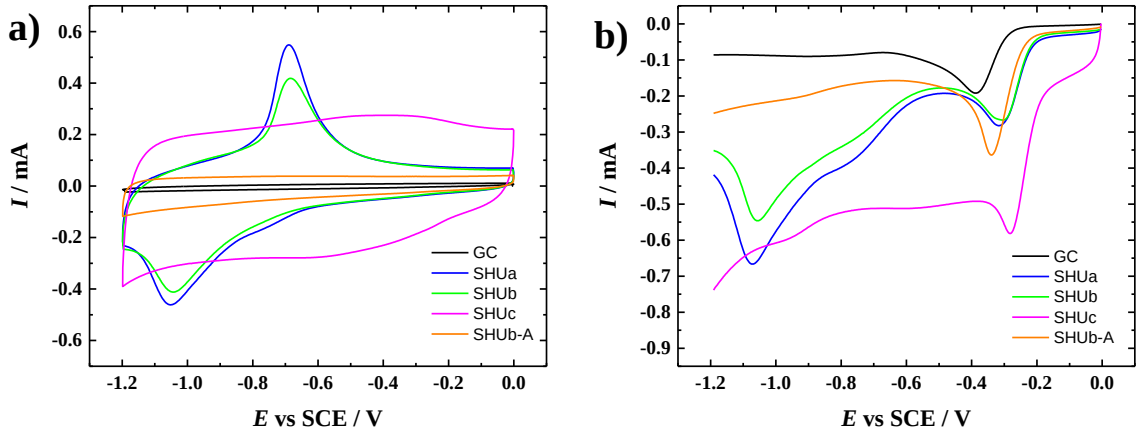

Figure 7. a) Cyclic voltammograms, b) linear sweep voltammograms of SHUa, SHUb(-A) and SHUc coated and bare GC electrodes recorded in a) Ar-saturated, b) O_2-saturated 0.1 M KOH solution using a potential scan rate of 100 mV s^{-1}.

In addition to CV, linear sweep voltammograms (LSVs) of GC coated with SHUa, SHUb, SHUb-A and SHUc materials and of bare GC electrode were recorded in O_2-saturated 0.1 M KOH solution. As expected, all materials exhibited higher electrocatalytic ORR activity than the bare GC electrode. Higher reduction current values for SHUa, SHUb(-A) and SHUc materials compared to GC have also a contribution from the larger capacitive currents as observed in the CVs in Figure 7a. Also, the reduction peak of Fe species is present in LSVs of SHUa and SHUb materials similarly as observed in the CV experiments. The ORR peak potential (E_p) values were determined from the LSV curves and are presented in Table 5. Among the different catalyst material coated electrodes, more positive E_p value was observed in case of SHUc referring to its better electrocatalytic activity towards ORR than the other materials.

The ORR performance was also studied in the hydrodynamic conditions using the RDE method. Baseline corrected RDE voltammetry curves of unmodified catalysts in comparison with commercial Pt/C recorded at 1900 rpm in O_2-saturated 0.1 M KOH solution are presented in Figure 8. Onset potential (E_{onset}) and O_2 reduction current at -0.5 V vs SCE were

determined and are shown in Table 5. Previous energy-related studies by Gusmão et al. that investigated shungite in comparison with other carbon-based materials showed superiority of shungite as a catalyst [3]. Catalytic activity of shungite materials in present study could be compared to that of the previously studied polymer-derived ceramic (PDC) electrocatalysts by our workgroup [44]. The PDC-based catalysts were employed also in a ball-milled powder form and had a very similar elemental composition. Moreover, SHUa and SHUb materials exhibited similar E_{onset} value of -0.21 V vs SCE, which is slightly better than that of GC/PDC-Co.

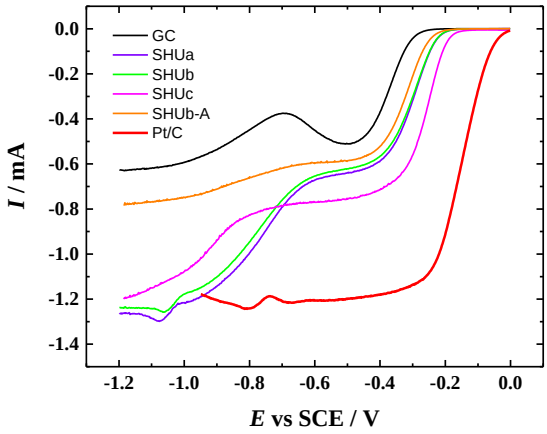

Figure 8. RDE voltammetry curves for oxygen reduction on bare and SHUa, SHUb, SHUb-A, SHUc and commercial Pt/C (20 µg cm^{-2}) catalyst coated GC electrodes in O_2-saturated 0.1 M KOH solution at 1900 rpm using a potential scan rate of 10 mV s^{-1}.

SHUb and SHUc materials were chosen for functionalisation with FePc and CoPc macrocyclic complexes. CVs and LSVs of these materials can be viewed in Figures 9a and b, respectively. As it can be seen from the CV curves, relatively smaller electroactive surface areas are observed with SHUc-based materials compared to their SHUb counterparts. Redox peaks of Fe are no longer observed in SHUb-Co/N, although in case of SHUb-Fe/N they are still present. Redox peaks are not present due to the removal of Fe by HF/HNO_3 leaching in case of SHUc-based materials. As can be seen from Figure 9b, SHUb-based materials resulted in more positive peak potentials, and therefore better ORR activity. This is a very interesting result as in case of unmodified materials, the SHUc was more active towards the ORR compared to the SHUb. As a possible explanation, we propose that in case of SHUc material, the HF/HNO_3 leaching functionalised the carbon material with N functionalities as observed in the EDX results (see Table 2). Therefore, in case of further modification with CoPc and FePc, lower amount of metal-Nx active sites for ORR could be imbedded into the SHUc

compared to the SHUb material as in case of SHUb no N was detected in its composition prior to functionalisation with metal phthalocyanines compounds (see Table 2).

Table 5. Peak potential (E_p), onset potential (E_{onset}), I at -0.5 V and half-wave potential ($E_{1/2}$) values for different catalyst material coated and bare GC electrode obtained in 0.1 M KOH.

Electrode	***E*p (V)**	E_{onset} **(V)**	$E_{1/2}$ **(V)**	***I* (mA)**
GC	-0.39	-0.28	–	-0.51
SHUa	-0.28	-0.21	–	-0.64
SHUb	-0.30	-0.21	–	-0.62
SHUb-A	-0.38	-0.23	–	-0.59
SHUc	-0.28	-0.17	–	-0.75
SHUb-Fe/N	-0.23	-0.06	-0.23	-1.02
SHUc-Fe/N	-0.35	-0.10	-0.21	-0.83
SHUb-Co/N	-0.26	-0.11	-0.25	-0.77
SHUc-Co/N	-0.27	-0.15	-0.28	-0.65
SHUb-Fe/N-A	-0.21	-0.07	-0.21	-1.03
SHUb-Co/N-A	-0.24	-0.08	-0.21	-0.89

The RDE voltammetry curves recorded at 1900 rpm with FePc and CoPc macrocyclic compound functionalised SHUb and SHUc material coated electrodes is presented in Figure 10 with a commercial Pt/C as a comparison. In addition to E_p, E_{onset} and I values, the half-wave potentials ($E_{1/2}$) were also determined from corresponding RDE voltammetry curves (see Table 5), and superior ORR activity of SHUb-based materials compared to SHUc counterparts was confirmed as in case of LSV experiments.

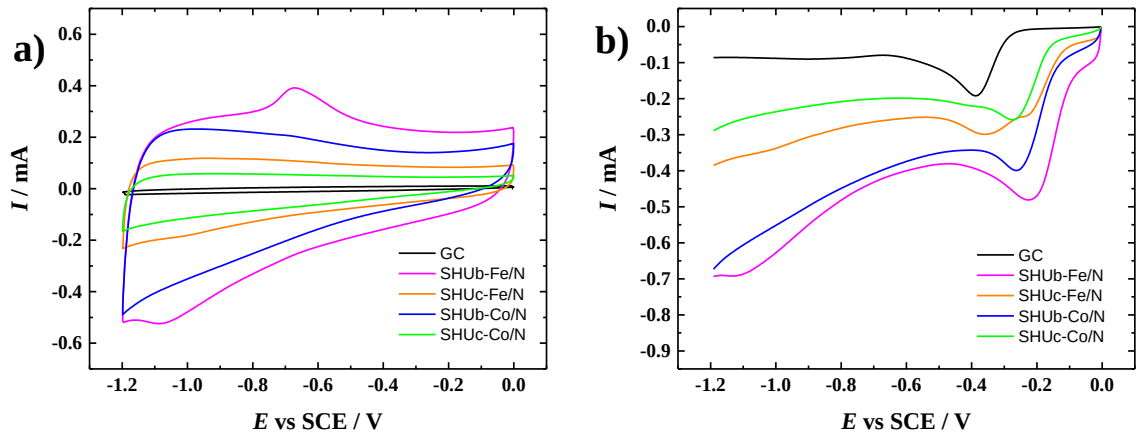

Figure 9. a) Cyclic voltammograms, b) linear sweep voltammograms of SHUb-Fe/N, SHUc-Fe/N, SHUb-Co/N and SHUc-Co/N material coated and bare GC electrodes recorded in a) Ar-saturated, b) O_2-saturated 0.1 M KOH solution using a potential scan rate of 100 mV s^{-1}.

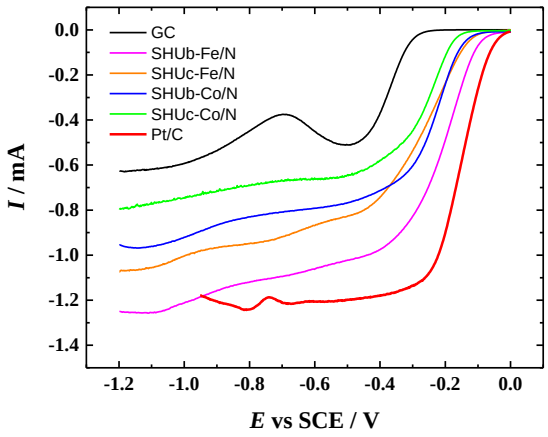

Figure 10. RDE voltammetry curves for oxygen reduction on bare and SHUb-Fe/N, SHUc-Fe/N, SHUb-Co/N, SHUc-Co/N and Pt/C (20 µg cm^{-2}) catalyst coated GC electrodes in O_2-saturated 0.1 M KOH solution at 1900 rpm using a potential scan rate of 10 mV s^{-1}.

Catalyst materials for further acid leaching were chosen to be SHUb-Fe/N and SHUb-Co/N, as they showed superior ORR activity compared to the SHUc-based counterparts. CVs and LSVs with corresponding acid treated and untreated material coated GC electrodes can be viewed in Figures 11a and b, respectively. In accordance with the EDX results obtained before and after acid leaching of SHUb material (see Table 2), the treatment has decreased Fe content in the FePc modified shungite according to the smaller Fe redox peaks observed from the polarisation curve of SHUb-Fe/N-A material compared to SHUb-Fe/N. Acid leaching has also contributed to more positive E_p (see Table 5), referring to an improved ORR performance.

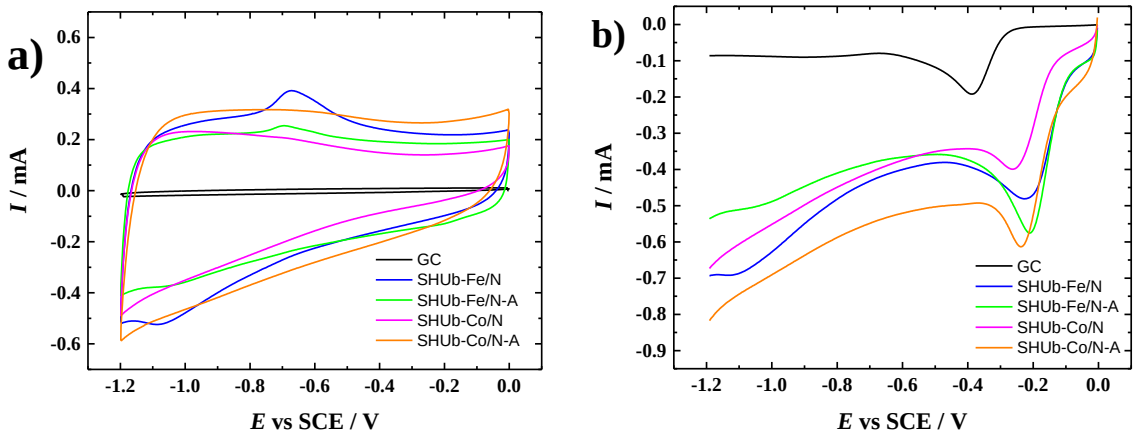

Figure 11. a) Cyclic voltammograms, b) linear sweep voltammograms of SHUb-Fe/N, SHUb-Fe/N-A, SHUb-Co/N and SHUb-Co/N-A material coated and bare GC electrodes recorded in a) Ar-saturated, b) O_2-saturated 0.1 M KOH using a scan rate of 100 mV s^{-1}.

The RDE method was also used for further investigation of the ORR activity of these materials and the RDE results in comparison with commercial Pt/C catalysts can be viewed in Figure 12. Similarly, E_p, E_{onset} and I and $E_{1/2}$ values were determined and may be viewed in Table 5. Most positive E_{onset} and $E_{1/2}$ were observed for SHUb-Fe/N-A and SHUb-Co/N-A catalyst. As mentioned before, the ORR activity of SHUb was similar to that of PDC-Co material from previous work by our group. The latter study showed, that introduction of nitrogen-containing groups in these materials improved the ORR activity, therefore PDC-Co-N material was found to be superior with an E_{onset} and $E_{1/2}$ of -0.1 and -0.38 V vs SCE respectively. The stability of PDC-Co-N during potential cycling in 0.1 M KOH was observed to be as good as Pt/C, therefore this material was regarded as an applicable ORR catalyst in microbial fuel cell [44]. Herein, the activities of PDC-Co-N and SHUb-Fe/N-A were compared, resulting in better ORR performance of shungite-based material, with more positive E_{onset} and $E_{1/2}$ values of -0.07 and -0.21 V vs SCE, respectively. Although, when compared to commercial Pt/C catalyst, the ORR activity of SHUb-Fe/N was still slightly lower.

As FePc modified shungite material remains superior to CoPc modified shungite, it is interesting to see how FePc modified CDC materials have performed in comparison with SHUb-Fe/N-A. The $E_{1/2}$ for O_2 reducion of FePc/CDC catalyst material was slightly lower than that of Pt/C. The catalyst showed ORR E_{onset} of -0.05 V vs SCE, just slightly more positive than SHUb-Fe/N-A (-0.07 V, see Table 5) [38]. Another study by our group of FePc modified CDC/CNT catalysts has found that, the ORR E_{onset} and $E_{1/2}$ for FePc modified CDC/CNT

composite catalyst is -0.08 V and -0.24 V vs SCE respectively, making shungite based material SHUb-Fe/N-A superior to the latter one [40].

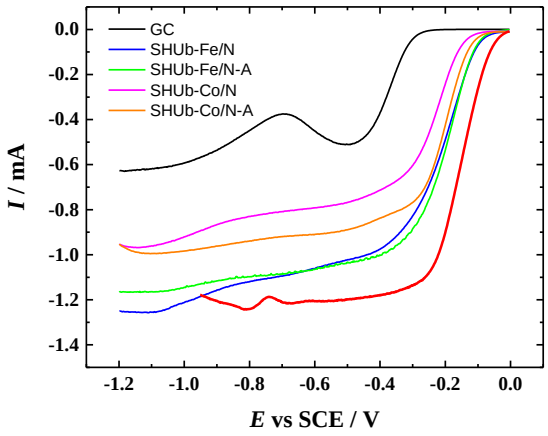

Figure 12. RDE voltammetry curves for oxygen reduction on bare and SHUb-Fe/N, SHUb-Fe/N-A, SHUb-Co/N, SHUb-Co/N-A and Pt/C (20 μg cm^{-2}) catalyst-coated GC electrodes in O_2-saturated 0.1 M KOH solution at 1900 rpm using a potential scan rate of 10 mV s^{-1}.

RDE polarisation curves at different rotation rates for the most active catalysts tested in 0.1 M KOH are presented in Figures 13a and c. From the RDE polarisation data, the number of electrons (n) per O_2 molecule were calculated using the Koutecky-Levich equation [57]:

3) $$\frac{1}{I} = \frac{1}{I_k} + \frac{1}{I_{dl}} = -\frac{1}{nFAkc_{O_2}^b} - \frac{1}{0{,}62nFAD_{O_2}^{2/3}v^{-1/6}c_{O_2}^b\omega^{1/2}}$$

Where I is the measured current, I_k and I_{dl} correspond to the kinetic and diffusion-limited currents respectively; k is the electrochemical rate constant for O_2 reduction; A is the geometric area of the electrode (0.196 cm^2); D is the diffusion coefficient of oxygen (1.9 × 10^5 cm^2 s^{-1}), c^b is its concentration in the bulk (1.2 × 10^{-6} mol cm^{-3}, v is the kinematic viscosity of the solution (0.01 cm^2 s^{-1}) [58,59]. These data are given for 0.1 M KOH solution. For the K-L analysis in 0.5 M H_2SO_4 solution, the following values for O_2 solubility (c^b = 1.13 × 10^{-6} mol cm^{-3}) and diffusion coefficient (D = 1.8 × 10^{-5} cm^2 s^{-1}) were used [60].

K–L plots were constructed and the n values were determined for the most active ORR catalyst and are presented in Figures 13b and d. According to the K–L plots, at lower overpotentials the oxygen reduction is under the mixed kinetic-diffusion control and at higher overpotentials parallel K–L lines yield intercepts by passing the origin of the axis, indicating that the oxygen reduction is limited by a mass transfer-diffusion to the electrode surface. The n value was calculated from the slopes of the K-L plots.

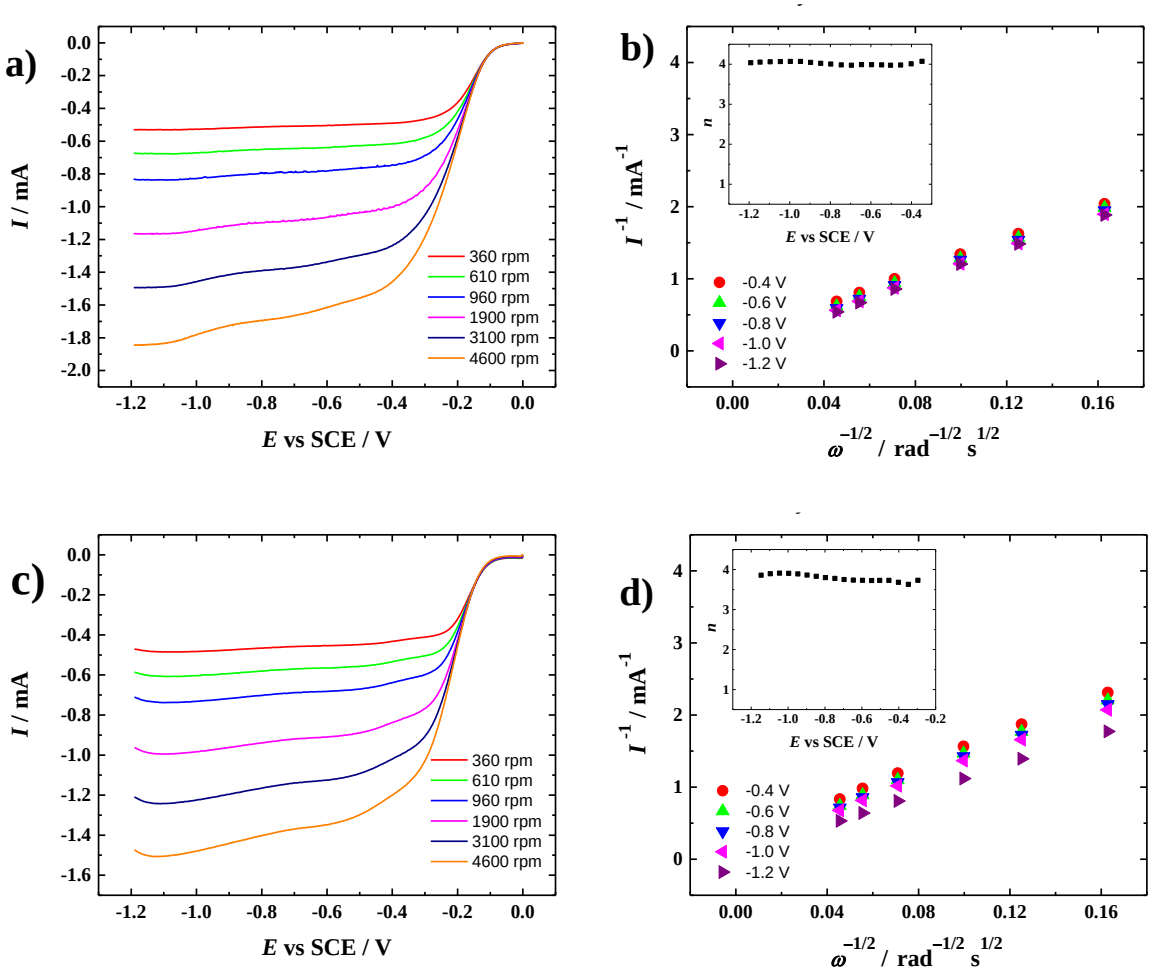

Figure 13. (a, c) RDE voltammetry curves for oxygen reduction in O_2-saturated 0.1 M KOH solution at different rotation rates using a scan rate of 10 mV s^{-1}; (b, d) K-L plots and number of electrons transferred per O_2 molecule for (a, b) SHUb-Fe/N-A, (c, d) SHUb-Co/N-A.

As mentioned, the electrocatalytic behaviour of the best performing ORR catalysts in the present work is quite similar to PDC-Co-N material from a previous study [44]. Herein, the highest *n* value of 4.0 was obtained for SHUb-Fe/N-A material, indicating the preferred $4e^-$ reduction pathway, which is also similar to the behaviour of the aforementioned GC/PDC-Co-N catalyst. Highest *n* value of 3.9 was achieved for SHUb-Co/N-A material. Therefore, both materials follow the favourable direct $4e^-$ or $2\times2e^-$ oxygen reduction pathways with OH^- as the final product in alkaline environment as shown in reactions 1a and 2a, b.

For practical application purposes of the catalysts at the fuel cell cathode, long-term stability of the catalyst during the ORR process was investigated. Stability testing was performed in O_2-saturated 0.1 M KOH similarly to the procedure from previous studies of our workgroup [61,62]. RDE polarisation curves were recorded at 960 rpm after every 100th CV curve, up to 2500 potential cycles and a selection of them can be viewed in Figure 14 for the electrodes

that exhibited the highest activity towards the ORR. In case of both electrodes, SHUb-Fe/N-A and SHUb-Co/N-A, after 2500 cycles, E_{onset} has not significantly changed, although the ORR current at -1.2 V has decreased by ca. 7-8 % compared to the initial value. Such behaviour is characteristic to the transition metal and N-doped carbon-based catalysts [63].

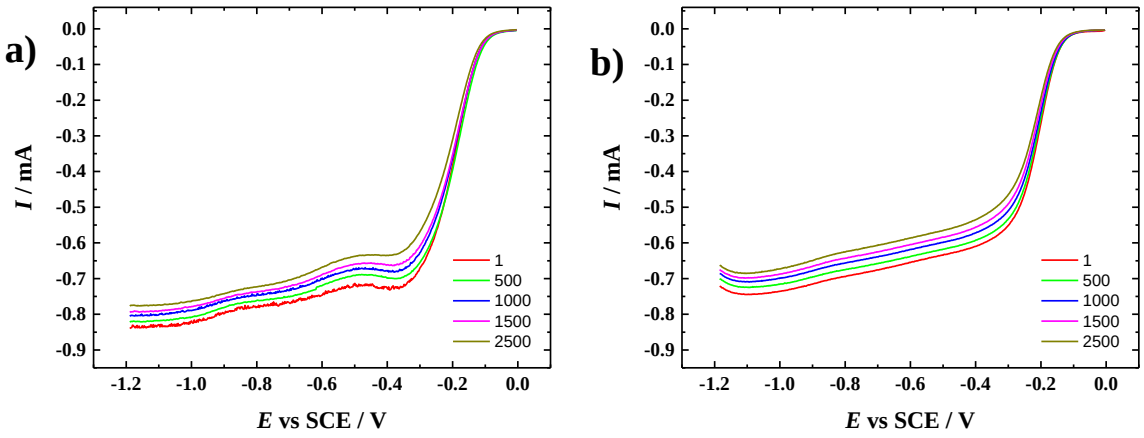

Figure 14. RDE voltammetry curves for oxygen reduction on a) SHUb-Fe/N-A and b) SHUb-Co/N-A electrodes recorded at 960 rpm after 1st, 500th, 1000th 1500th and 2500th potential cycles in O_2-saturated 0.1 M KOH solution, scan rate 10 mV s^{-1}.

From the studied materials in 0.1 M KOH solution, SHUb-Fe/N-A and SHUb-Co/N-A exhibit the best ORR performance, making them suitable for possible future testing as a cathode catalyst in the AEMFC.

4.2.2 ORR studies in 0.5 M H_2SO_4 solution

FePc and CoPc modified SHUb and SHUc materials were also subjected to ORR studies in acidic media. In order to assess the electrochemical behaviour of these materials in the absence of O_2, CVs were recorded in Ar-saturated 0.5 M H_2SO_4 solution. As it can be seen from Figure 15a, the highest capacitive current is observed for SHUb-Co/N, while the lowest for SHUc-Co/N material coated GC electrode. In case of their FePc-based counterparts, corresponding difference is considerably smaller. Redox peaks of Fe are still present at around 0.4 V SCE in the anodic and cathodic scans for all materials, except SHUc-Co/N. According to the literature, this redox wave could correspond to the Fe^{2+}/Fe^{3+} redox transition [64,65]. From the LSV curves presented in Figure 15b, the E_p values were determined and are listed in Table 6.

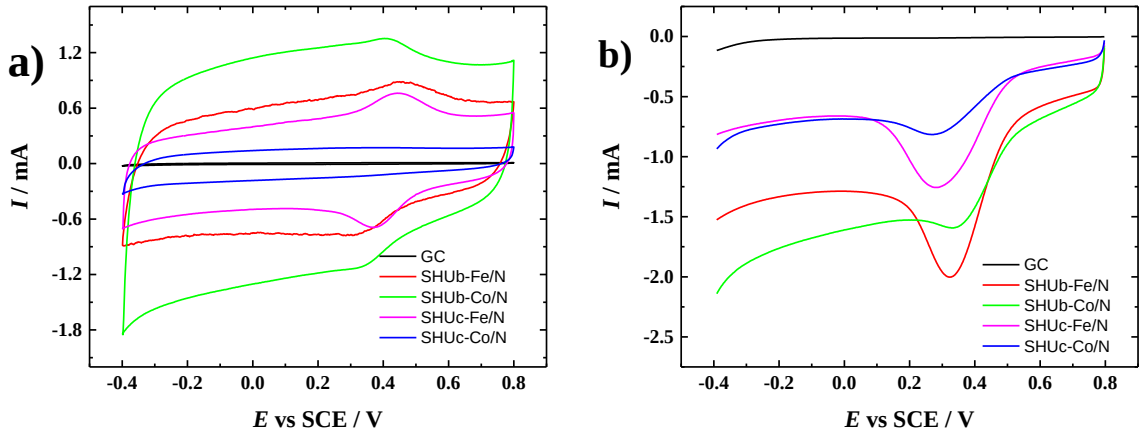

Figure 15. a) Cyclic voltammograms, b) linear sweep voltammograms of SHUb-Fe/N, SHUc-Fe/N, SHUb-Co/N and SHUc-Co/N material coated and bare GC electrodes recorded in a) Ar-saturated, b) O_2-saturated 0.5 M H_2SO_4 solution using a scan rate of 100 mV s^{-1}.

As it can be seen, SHUb-based materials expressed more positive E_p, and therefore, a better ORR electrocatalytic activity. In order to confirm the superiority of SHUb-based materials, RDE measurements were also conducted in O_2-saturated 0.5 M H_2SO_4 solution and corresponding RDE polarisation curves can be viewed in Figure 16. As expected, SHUb-Fe/N and SHUb-Co/N showed higher ORR activity compared to their SHUc-based counterparts in terms of E_{onset} and $E_{1/2}$ values that are presented in Table 6. Based on the RDE results, the advantage of SHUb-based materials was assured. Since the acid-treated materials showed the best performance in alkaline solution, it was also interesting to see how these materials would behave in acidic medium. It has been established that N-doped carbon nanomaterials are highly active in alkaline medium and show poor ORR activity in acidic environment. Although, there has not been a suitable approach for understanding the nature and the reaction mechanism of M/N/C catalysts; the origin of such pH-dependent activity still remains unclear, making the rational design of the ORR electrocatalyst more difficult [1,21,66]. Therefore, the electrocatalytic ORR activity of pristine SHUb-based FePc and CoPc was compared to that of their corresponding acid leached counterparts. CVs of pristine and acid leached SHUb-based FePc and CoPc modified materials are presented in Figure 17a.

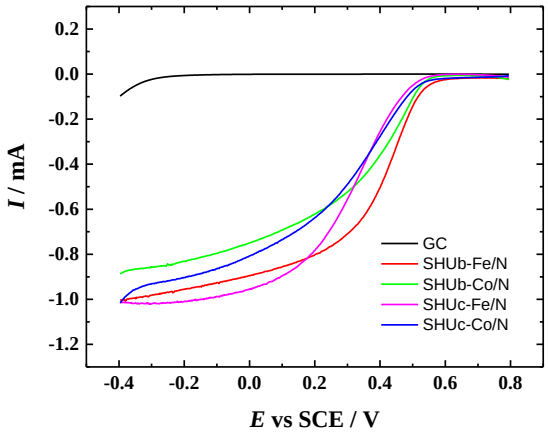

Figure 16. RDE voltammetry curves for oxygen reduction on SHUb-Fe/N, SHUc-Fe/N-A, SHUb-Co/N and SHUc-Co/N coated and bare GC electrodes recorded in O_2-saturated 0.5 M H_2SO_4 solution at 1900 rpm using a potential scan rate of 10 mV s^{-1}.

Table 6. ORR peak potential (E_p), onset potential (E_{onset}), I at -0.2 V and half-wave potential ($E_{1/2}$) values determined for different catalyst material coated and bare GC electrodes in O_2 saturated 0.5 M H_2SO_4 solution.

Electrode	E_p (V)	E_{onset} (V)	$E_{1/2}$ (V)	I (mA)
GC	–	-0.32	-	-
SHUb-Fe/N	0.32	0.58	0.40	-0.96
SHUc-Fe/N	0.28	0.52	0.32	-1.01
SHUb-Co/N	0.33	0.54	0.36	-0.83
SHUc-Co/N	0.27	0.55	0.30	-0.90
SHUb-Fe/N-A	0.26	0.54	0.39	-0.93
SHUb-Co/N-A	0.31	0.55	0.38	-0.85

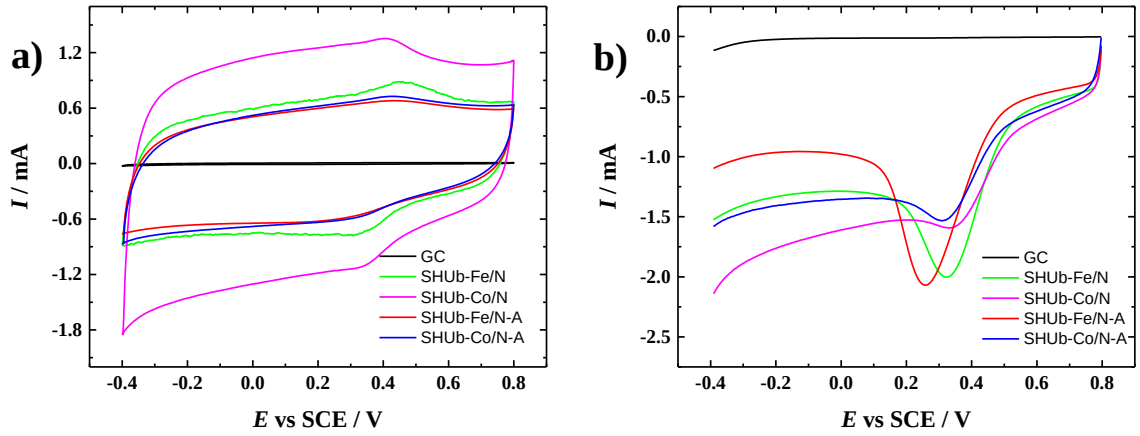

Figure 17. a) Cyclic voltammograms, b) linear sweep voltammograms of SHUb-Fe/N, SHUb-Fe/N-A, SHUb-Co/N and SHUb-Co/N-A material coated and bare GC electrodes recorded in a) Ar-saturated, b) O_2-saturated 0.5 M H_2SO_4 solution at a scan rate of 100 mV s^{-1}.

Small Fe redox peaks on CVs are still observed in case of acid-treated catalyst materials in Ar-saturated 0.5 M H_2SO_4 solution. LSV curves are presented in Figure 17b and the E_p values for these materials are presented in Table 6. More positive E_p values are interestingly observed for materials that were not acid-treated. The RDE results presented in Figure 18 ascertain a better ORR activity of the SHUb-Fe/N electrode compared to the SHUb-Fe/N-A according to the values of E_{onset} and $E_{1/2}$ (see Table 6). The SHUb-Fe/N exhibits the highest activity towards the ORR in 0.5 M H_2SO_4 among all the catalysts studied in this work.

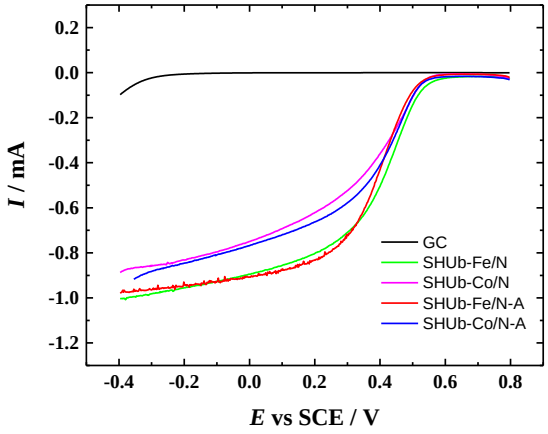

Figure 18. RDE voltammetry curves for oxygen reduction on SHUb-Fe/N, SHUb-Fe/N-A, SHUb-Co/N and SHUb-Co/N-A coated and bare GC electrodes recorded in O_2-saturated 0.5 M H_2SO_4 solution at 1900 rpm using a potential scan rate of 10 mV s^{-1}.

As discussed about the ORR results obtained in alkaline solution, comparable E_{onset} and $E_{1/2}$ values were observed with CDC/CNT/CoPc and CDC/CNT/FePc catalysts from previous

studies by our workgroup. Electrocatalytic activities of these materials were also explored in 0.5 M H_2SO_4 solution; therefore, it is appropriate to have the results compared to the shungite-based materials. CoPc modified CDC/CNT composite materials have been reported to achieve onset potential of 0.53 V vs SCE and $E_{1/2}$ of 0.38 V vs SCE and as can be seen from Table 6, corresponding values of SHUb-Co/N and SHUb-Co/N-A materials are more positive, therefore they exhibit better ORR activity [41]. As for the best performing CDC/CNT modified with FePc, E_{onset} of 0.59 V and $E_{1/2}$ of 0.42 V vs SCE was achieved in acidic media, which are still slightly more positive than that of the corresponding FePc modified shungite materials [40].

Figures 19a and c depict the RDE polarisation curves at different rotation rates for SHUb-Fe/N and SHUb-Co/N catalyst materials. Also, the K-L plots with the insets presenting the electron transfer number are shown for corresponding electrodes in Figures 19b and d. The Fe-based material exhibits the *n* value between 2 and 4, with a maximum of 3.7. As for the Co-based material, corresponding value is higher throughout the studied potential range achieving the highest value of 3.9. The ORR on SHUb-Co/N material could more likely follow the favourable direct $4e^-$ oxygen reduction as depicted by reaction 1b. While, SHUb-Fe/N material follows the mixed $2\times2e^-$ pathway yielding both peroxide and H_2O as final products as depicted by reactions 2c and d. The value of *n* increases at more negative potentials indicating water being the main product of the ORR process together with only a small amount of peroxide. Based on the results obtained herein, great potential of shungite-based materials make them attractive as cathode catalysts for PEMFC application. The most important reasons behind the high ORR activity of the FePc- and CoPc-modified catalyst materials in both acidic and alkaline environment are most likely the pyridinic-N and metal-Nx active sites embedded into the shungite material during pyrolysis as ascertained with the presence of transition metal and N species by XRD and XPS analysis (see Section 4.1) [2,34,36,67,68].

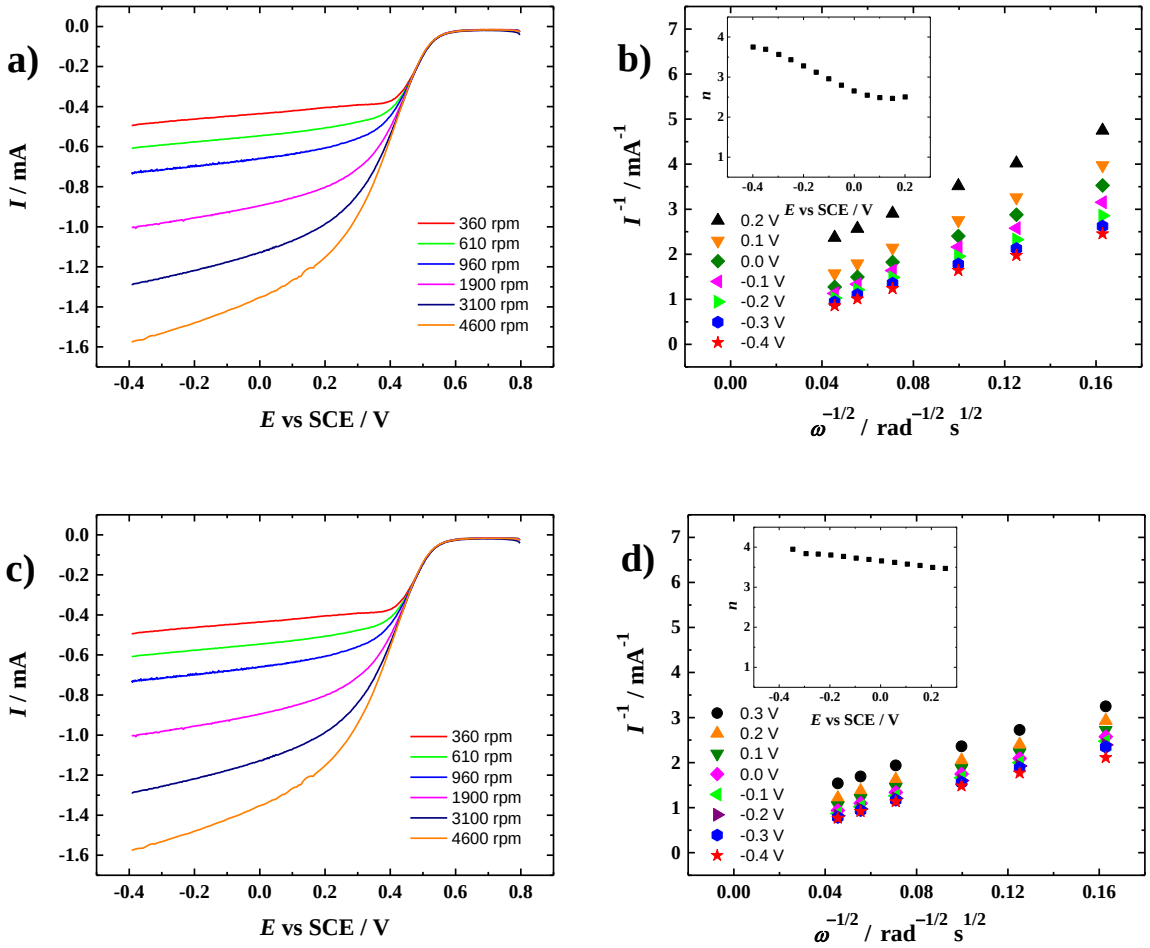

Figure 19. (a, c) RDE voltammetry curves for oxygen reduction recorded in O_2-saturated 0.5 M H_2SO_4 solution at different rotation rates at scan rate of 10 mV s^{-1}; (b, d) K-L plots and number of electrons transferred per O_2 molecule for (a, b) SHUb-Fe/N, (c, d) SHUb-Co/N.

4.2.3 OER studies in 0.1 M KOH solution

In addition to studying electrocatalytic ORR activity of shungite-based catalysts in this work, the OER was also investigated, as this reaction is an important half-reaction involved in water electrolysis, with its main applications in rechargeable metal-air batteries, although active sites responsible for OER, are not the same as sites required for ORR. The OER activity of shungite in this study was compared to that of previously assessed energy related applications of shungite in comparison with other carbon materials, where shungite was reported as a reliable OER catalyst [3]. The $E_{j=10}$ of 0.09 V vs SCE (determined at 10 mA cm^{-2}) was obtained for pristine shungite in 1 M KOH solution.

In order to assess the overall bifunctional oxygen activity (ΔE), potential differences between $E_{j=10}$ for OER and $E_{1/2}$ for ORR was calculated ($\Delta E = E_{j=10} - E_{1/2}$). The OER polarisation curves were recorded in Ar-saturated 0.1 M KOH solution and are presented in Figure 20. The only electrode achieving $E_{j=10}$ at 2 mA (equal to 10 mA cm^{-2}) is SHUb-Co/N ($E_{j=10}$ = 0.79 V vs SCE, $E_{1/2}$ is -0.25 V vs SCE) so ΔE of 1.04 V was determined for this material. Other materials were simply not active enough for OER to achieve 2 mA current in the studied potential range.

Study by Ping et al. of bifunctional oxygen electrocatalyst has reported an excellent bifunctional behaviour of ORR/OER, ΔE = 0.73 V in 0.1 M KOH for iron/benzimidazole-based metal-organic-framework material [69]. As the data for ORR and OER measurements was automatically corrected for iR drop using the Nova software in latter study [69], the corresponding data correction was also carried out for the ΔE value determination of SHUb-Co/N herein to make the conditions similar for the comparison. The R value of 48 Ω was obtained from the electrochemical impedance spectroscopy for ORR reaction at constant potential of -1.1 V in O_2-saturated 0.1 M KOH. The ΔE value improved by -0.11 V to 0.93 V due to iR drop correction, where the difference is mainly due to the corrected OER $E_{j=10}$ value (0.69 V). Considering these findings, iR drop correction is very important when the OER is evaluated as it considerably improved the OER $E_{j=10}$ value. By comparing ΔE value obtained herein with one from Ping et al. work, it was clear that the shungite catalyst materials prepared in this work would need further development to meet the standard of a successful bifunctional electrocatalyst [69].

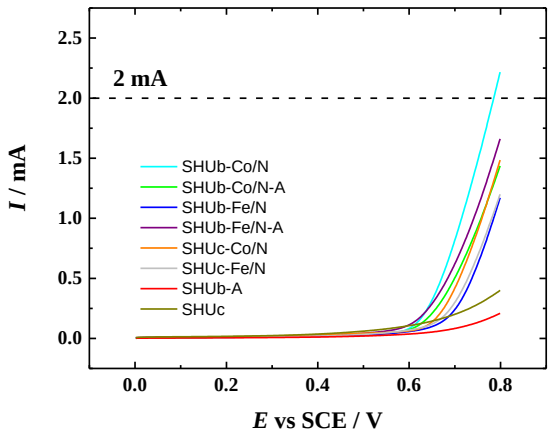

Figure 20. OER polarisation curves on different catalyst-coated GC electrodes recorded in Ar-saturated 0.1 M KOH solution at 1900 rpm at a scan rate of 10 mV s^{-1}.

SUMMARY

Electrochemical investigation of electrocatalytic oxygen reduction and oxygen evolution reactions was performed with FePc and CoPc modified natural shungite material in alkaline and acidic environments using CV, LSV and RDE methods. Shungite materials were functionalised with metal phthalocyanines via high-temperature pyrolysis in an inert atmosphere.

Surface morphology of the electrocatalysts was evaluated using SEM-EDX, XRD, XPS and Raman spectroscopy, indicating successful functionalisation with the transition metal macrocyclic complexes. Most importantly, the XPS results showed evidence for the metal-Nx and pyridinic-N species, which are considered highly beneficial for ORR electrocatalysis. In addition, the presence of transition metals from phthalocyanine complexes was ascertained by XPS and XRD analysis.

Electrochemical studies in 0.1 M KOH solution showed superior oxygen reduction performance of the acid-treated FePc-modified shungite with the preferred $4e^-$ reduction pathway and the $E_{1/2}$ value of -0.21 V vs SCE. In the RDE study conducted in 0.5 M H_2SO_4 solution, FePc modified KOH-treated shungite resulted in the highest ORR activity according to the $E_{1/2}$ value (0.40 V vs SCE). Compared to the latter, the CoPc-based counterpart showed an electron transfer number closer to $4e^-$ and a slightly lower $E_{1/2}$ of 0.36 V vs SCE. The bifunctionality of Co-based material was evaluated in 0.1 M KOH showing ΔE of 0.93 V vs SCE (value obtained with iR drop correction of the *I-E* curves for ORR and OER).

To summarise, based on the results obtained from physical and electrochemical characterisations of the prepared electrocatalysts, most active materials would be appealing to be employed as ORR cathode catalyst for the AEMFC and PEMFC applications.

REFERENCES

[1] A. Sarapuu, E. Kibena-Põldsepp, M. Borghei, K. Tammeveski, Electrocatalysis of oxygen reduction on heteroatom-doped nanocarbons and transition metal–nitrogen–carbon catalysts for alkaline membrane fuel cells, J. Mater. Chem. A 6 (2018) 776–804. https://doi.org/10.1039/C7TA08690C.

[2] Y. Zhao, G. Yu, F. Wang, P. Wei, J. Liu, Bioinspired Transition-Metal Complexes as Electrocatalysts for the Oxygen Reduction Reaction, Chem. Eur. J. 25 (2019) 3726–3739. https://doi.org/10.1002/chem.201803764.

[3] R. Gusmão, Z. Sofer, D. Bouša, M. Pumera, Synergetic Metals on Carbocatalyst Shungite, Chem. Eur. J. 23 (2017) 18232–18238. https://doi.org/10.1002/chem.201703974.

[4] I. Kruusenberg, L. Matisen, Q. Shah, A.M. Kannan, K. Tammeveski, Non-platinum cathode catalysts for alkaline membrane fuel cells, Int. J. Hydrog. Energy 37 (2012) 4406–4412. https://doi.org/10.1016/j.ijhydene.2011.11.143.

[5] S.Y. Chazhengina, V.V. Kovalevski, Structural characteristics of shungite carbon subjected to contact metamorphism overprinted by greenschist-facies regional metamorphism, Eur. J. Mineral. 25 (2014) 835–843. https://doi.org/10.1127/0935-1221/2013/0025-2327.

[6] N. Daems, X. Sheng, I.F.J. Vankelecom, P.P. Pescarmona, Metal-free doped carbon materials as electrocatalysts for the oxygen reduction reaction, J. Mater. Chem. A 2 (2014) 4085–4110. https://doi.org/10.1039/C3TA14043A.

[7] L. Parfeneva, T. Volkonskaya, V. Tikhonov, I. Kulikova, I. Smirnov, N. Rozhkova, A. Zaidenberg, Thermal conductivity, heat capacity, and thermoelectric power of schungite carbon, Phys. Solid State 36 (1994) 625–627.

[8] V.A. Reznikov, Yu.S. Polekhovskii, Amorphous shungite carbon: A natural medium for the formation of fullerenes, Tech. Phys. Lett. 26 (2000) 689–693. https://doi.org/10.1134/1.1307814.

[9] M. Mastalerz, M. Glikson, B.A. Stankiewicz, I.B. Volkova, R.M. Bustin, Organic and mineral matter in a Precambrian shungite deposit from Karelia, Russia, in: M. Glikson, M. Mastalerz (Eds.), Organic Matter and Mineralisation: Thermal Alteration, Hydrocarbon Generation and Role in Metallogenesis, Springer Netherlands, Dordrecht, 2000: pp. 102–119. https://doi.org/10.1007/978-94-015-9474-5_6.

[10] S.V. Efremova, Water treatment with a shungite sorbent and biosorbents on its base, Russ. J. Appl. Chem. 79 (2006) 397–402. https://doi.org/10.1134/S1070427206030128.

[11] S.A. Efremov, S.V. Nechipurenko, M. Kazankapova, W. Braida, Kh.S. Tassibekov, M. Nauryzbayev, Physico-Chemical Characteristics of Shungite Rock of Kazakhstan, Eurasian Chem.-Technol. J. 15 (2013) 241–249. https://doi.org/10.18321/ectj228.
[12] M.V. Charykova, I.I. Bornyakova, Yu.S. Polekhovskii, N.A. Charykov, E.V. Kustova, O.V. Arapov, Chemical composition of extracts from shungite and "shungite water," Russ. J. Appl. Chem. 79 (2006) 29–33. https://doi.org/10.1134/S107042720601006X.
[13] P.R. Buseck, L.P. Galdobina, V. Kovalevski, N. Rozhkova, J. Valley, A.Z. Zaidenberg, Shungites: The C-rich rocks of Karelia, Russia, Can. Mineral. 35 (1997) 1363–1378.
[14] V. Sokolov, Y.K. Kalinin, E. Dyukkiev, Shungity—novoe uglerodistoe syr'e, (1984).
[15] S.V. Krasnovyd, A.A. Konchits, B.D. Shanina, M.Y. Valakh, I.B. Yanchuk, V.O. Yukhymchuk, A.V. Yefanov, M.A. Skoryk, Local structure and paramagnetic properties of the nanostructured carbonaceous material shungite, Nanoscale Res. Lett. 10 (2015) 78. https://doi.org/10.1186/s11671-015-0767-9.
[16] S. Oliynyk, L. Mel'nyk, I. Samchenko, N. Tkachuk, O. Loginova, L. Kisterska, Influence of shungite treatment methods on its absorption properties and on water treatment quality for beverages production, Ukr. Food J. 8 (2019) 891–902. https://doi.org/10.24263/2304-974X-2019-8-4-18.
[17] O. Selinus, R.B. Finkelman, J.A. Centeno, Medical Geology: A Regional Synthesis, Springer Science & Business Media, 2010.
[18] R. Sibul, E. Kibena-Põldsepp, S. Ratso, M. Kook, M.T. Sougrati, M. Käärik, M. Merisalu, J. Aruväli, P. Paiste, A. Treshchalov, J. Leis, V. Kisand, V. Sammelselg, S. Holdcroft, F. Jaouen, K. Tammeveski, Iron- and Nitrogen-Doped Graphene-Based Catalysts for Fuel Cell Applications, ChemElectroChem 7 (2020) 1739–1747. https://doi.org/10.1002/celc.202000011.
[19] D.R. Dekel, Review of cell performance in anion exchange membrane fuel cells, J. Power Sources 375 (2018) 158–169. https://doi.org/10.1016/j.jpowsour.2017.07.117.
[20] S.J. Peighambardoust, S. Rowshanzamir, M. Amjadi, Review of the proton exchange membranes for fuel cell applications, Int. J. Hydrog. Energy 35 (2010) 9349–9384. https://doi.org/10.1016/j.ijhydene.2010.05.017.
[21] X. Zhang, C. Chen, J. Dong, R.-X. Wang, Q. Wang, Z.-Y. Zhou, S.-G. Sun, Comparative Study of the Oxygen Reduction Reaction on Pyrolyzed FePc in Acidic and Alkaline Media, ChemElectroChem 5 (2018) 3946–3952. https://doi.org/10.1002/celc.201801179.

[22] L. Ma, S. Chen, Z. Pei, Y. Huang, G. Liang, F. Mo, Q. Yang, J. Su, Y. Gao, J.A. Zapien, C. Zhi, Single-Site Active Iron-Based Bifunctional Oxygen Catalyst for a Compressible and Rechargeable Zinc–Air Battery, ACS Nano 12 (2018) 1949–1958. https://doi.org/10.1021/acsnano.7b09064.

[23] Y. Li, M. Gong, Y. Liang, J. Feng, J.-E. Kim, H. Wang, G. Hong, B. Zhang, H. Dai, Advanced zinc-air batteries based on high-performance hybrid electrocatalysts, Nat. Commun. 4 (2013) 1–7. https://doi.org/10.1038/ncomms2812.

[24] S. Sui, X. Wang, X. Zhou, Y. Su, S. Riffat, C. Liu, A comprehensive review of Pt electrocatalysts for the oxygen reduction reaction: Nanostructure, activity, mechanism and carbon support in PEM fuel cells, J. Mater. Chem. A 5 (2017) 1808–1825. https://doi.org/10.1039/C6TA08580F.

[25] Z. Liang, H. Zheng, R. Cao, Importance of Electrocatalyst Morphology for the Oxygen Reduction Reaction, ChemElectroChem 6 (2019) 2600–2614. https://doi.org/10.1002/celc.201801859.

[26] A. Elzing, A. van der Putten, W. Visscher, E. Barendrecht, The cathodic reduction of oxygen at cobalt phthalocyanine, J. Electroanal. Chem. Interfacial Electrochem. 200 (1986) 313–322. https://doi.org/10.1016/0022-0728(86)90063-X.

[27] G.-L. Chai, Z. Hou, T. Ikeda, K. Terakura, Two-Electron Oxygen Reduction on Carbon Materials Catalysts: Mechanisms and Active Sites, J. Phys. Chem. C 121 (2017) 14524–14533. https://doi.org/10.1021/acs.jpcc.7b04959.

[28] B. Wang, Recent development of non-platinum catalysts for oxygen reduction reaction, J. Power Sources 152 (2005) 1–15. https://doi.org/10.1016/j.jpowsour.2005.05.098.

[29] X. Wang, C. Ouyang, S. Dou, D. Liu, S. Wang, Oxidized carbon nanotubes as an efficient metal-free electrocatalyst for the oxygen reduction reaction, RSC Adv. 5 (2015) 41901–41904. https://doi.org/10.1039/C5RA05172J.

[30] L. Khotseng, Oxygen Reduction Reaction, Electrocatalysts for Fuel Cells and Hydrogen Evolution - Theory to Design (2018). https://doi.org/10.5772/intechopen.79098.

[31] N.B. McKeown, Phthalocyanines, in: J.A. McCleverty, T.J. Meyer (Eds.), Comprehensive Coordination Chemistry II, Pergamon, Oxford, 2003: pp. 507–514. https://doi.org/10.1016/B0-08-043748-6/01071-9.

[32] Phthalocyanine, Am. Chem. Soc. (n.d.). https://www.acs.org/content/acs/en/molecule-of-the-week/archive/p/phthalocyanine.html (accessed May 13, 2020).

[33] K. Tammeveski, J.-S. Yu, Z. Chen, Non-Precious-Metal Oxygen Reduction Reaction Electrocatalysis, ChemElectroChem 5 (2018) 1743–1744.

https://doi.org/10.1002/celc.201800751.
[34] Y. Liu, X. Yue, K. Li, J. Qiao, D.P. Wilkinson, J. Zhang, PEM fuel cell electrocatalysts based on transition metal macrocyclic compounds, Coord. Chem. Rev. 315 (2016) 153–177. https://doi.org/10.1016/j.ccr.2016.02.002.
[35] E. Lam, J.H.T. Luong, Carbon Materials as Catalyst Supports and Catalysts in the Transformation of Biomass to Fuels and Chemicals, ACS Catal. 4 (2014) 3393–3410. https://doi.org/10.1021/cs5008393.
[36] K. Tammeveski, J.H. Zagal, Electrocatalytic oxygen reduction on transition metal macrocyclic complexes for anion exchange membrane fuel cell application, Curr. Opin. Electrochem. 9 (2018) 207–213. https://doi.org/10.1016/j.coelec.2018.04.001.
[37] I. Kruusenberg, J. Mondal, L. Matisen, V. Sammelselg, K. Tammeveski, Oxygen reduction on graphene-supported MN_4 macrocycles in alkaline media, Electrochem. Commun. 33 (2013) 18–22. https://doi.org/10.1016/j.elecom.2013.04.005.
[38] R. Praats, I. Kruusenberg, M. Käärik, U. Joost, J. Aruväli, P. Paiste, R. Saar, P. Rauwel, M. Kook, J. Leis, J.H. Zagal, K. Tammeveski, Electroreduction of oxygen in alkaline solution on iron phthalocyanine modified carbide-derived carbons, Electrochim. Acta 299 (2019) 999–1010. https://doi.org/10.1016/j.electacta.2019.01.062.
[39] K.-K. Türk, I. Kruusenberg, J. Mondal, P. Rauwel, J. Kozlova, L. Matisen, V. Sammelselg, K. Tammeveski, Oxygen electroreduction on MN_4-macrocycle modified graphene/multi-walled carbon nanotube composites, J. Electroanal. Chem. 756 (2015) 69–76. https://doi.org/10.1016/j.jelechem.2015.08.014.
[40] R. Praats, M. Käärik, A. Kikas, V. Kisand, J. Aruväli, P. Paiste, M. Merisalu, J. Leis, V. Sammelselg, J.H. Zagal, S. Holdcroft, N. Nakashima, K. Tammeveski, Electrocatalytic oxygen reduction reaction on iron phthalocyanine-modified carbide-derived carbon/carbon nanotube composite electrocatalysts, Electrochim. Acta 334 (2020) 135575. https://doi.org/10.1016/j.electacta.2019.135575.
[41] R. Praats, M. Käärik, A. Kikas, V. Kisand, J. Aruväli, P. Paiste, M. Merisalu, A. Sarapuu, J. Leis, V. Sammelselg, J.C. Douglin, D.R. Dekel, K. Tammeveski, Electroreduction of oxygen on cobalt phthalocyanine-modified carbide-derived carbon/carbon nanotube composite catalysts, J. Solid State Electrochem. (2020). https://doi.org/10.1007/s10008-020-04543-z.
[42] K. Liu, S. Kattel, V. Mao, G. Wang, Electrochemical and Computational Study of Oxygen Reduction Reaction on Nonprecious Transition Metal/Nitrogen Doped Carbon Nanofibers in Acid Medium, J. Phys. Chem. C 120 (2016) 1586–1596.

https://doi.org/10.1021/acs.jpcc.5b10334.
[43] R. Chen, H. Li, D. Chu, G. Wang, Unraveling Oxygen Reduction Reaction Mechanisms on Carbon-Supported Fe-Phthalocyanine and Co-Phthalocyanine Catalysts in Alkaline Solutions, J. Phys. Chem. C 113 (2009) 20689–20697. https://doi.org/10.1021/jp906408y.
[44] T.C. de A. e Silva, M. Mooste, E. Kibena-Põldsepp, L. Matisen, M. Merisalu, M. Kook, V. Sammelselg, K. Tammeveski, M. Wilhelm, K. Rezwan, Polymer-derived Co/Ni–SiOC(N) ceramic electrocatalysts for oxygen reduction reaction in fuel cells, Catal. Sci. Technol. 9 (2019) 854–866. https://doi.org/10.1039/C8CY02207K.
[45] D. Bossert, D.A. Urban, M. Maceroni, L. Ackermann-Hirschi, L. Haeni, P. Yajan, M. Spuch-Calvar, B. Rothen-Rutishauser, L. Rodriguez-Lorenzo, A. Petri-Fink, F. Schwab, A hydrofluoric acid-free method to dissolve and quantify silica nanoparticles in aqueous and solid matrices, Sci. Rep. 9 (2019) 7938. https://doi.org/10.1038/s41598-019-44128-z.
[46] M. Steinert, J. Acker, S. Oswald, K. Wetzig, Study on the Mechanism of Silicon Etching in HNO_3-Rich HF/HNO_3 Mixtures, J. Phys. Chem. C 111 (2007) 2133–2140. https://doi.org/10.1021/jp066348j.
[47] S. Ratso, I. Kruusenberg, A. Sarapuu, P. Rauwel, R. Saar, U. Joost, J. Aruväli, P. Kanninen, T. Kallio, K. Tammeveski, Enhanced oxygen reduction reaction activity of iron-containing nitrogen-doped carbon nanotubes for alkaline direct methanol fuel cell application, J. Power Sources 332 (2016) 129–138. https://doi.org/10.1016/j.jpowsour.2016.09.069.
[48] N. Obradović, M. Gigov, A. Djordjevic, F. Kern, S. Butulija, B. Matovic, A. Đordjevic, A. Tshantshapanyan, B. Vlahovic, P. Petrovic, V. Pavlovic, Shungite - a carbon-mineral rock material: Its sinterability and possible applications, Process. Appl. Ceram. 13 (2019) 89–97. https://doi.org/10.2298/PAC1901089O.
[49] E. Bilgin Simsek, Z. Balta, P. Demircivi, Novel shungite based Bi2WO6 carbocatalyst with high photocatalytic degradation of tetracycline under visible light irradiation, J. Photochem. Photobiol. Chem. 380 (2019) 111849. https://doi.org/10.1016/j.jphotochem.2019.05.012.
[50] M.S. Seehra, U.K. Geddam, D. Schwegler-Berry, A.B. Stefaniak, Detection and quantification of 2H and 3R phases in commercial graphene-based materials, Carbon 95 (2015) 818–823. https://doi.org/10.1016/j.carbon.2015.08.109.
[51] B. Dippel, H. Jander, J. Heintzenberg, NIR FT Raman spectroscopic study of flame soot, Phys. Chem. Chem. Phys. 1 (1999) 4707–4712. https://doi.org/10.1039/A904529E.

[52] R. Morga, About the Microstructure of the Graptolite Periderm - Examples from the Holy Cross Mountains (Poland), IOP Conf. Ser. Earth Environ. Sci. 362 (2019) 012076. https://doi.org/10.1088/1755-1315/362/1/012076.
[53] Y. Golubev, S. Isaenko, A. Prikhodko, N. Borgardt, E. Suvorova, Raman spectroscopic study of natural nanostructured carbon materials: shungite vs. anthraxolite, Eur. J. Mineral. 3 (2016) 545–554. https://doi.org/10.1127/ejm/2016/0028-2537.
[54] S. Arunmetha, A. Karthik, S.R. Srither, M. Vinoth, R. Suriyaprabha, P. Manivasakan, V. Rajendran, Size-dependent physicochemical properties of mesoporous nanosilica produced from natural quartz sand using three different methods, RSC Adv. 5 (2015) 47390–47397. https://doi.org/10.1039/C5RA07074K.
[55] X. Ning, Y. Li, J. Ming, Q. Wang, H. Wang, Y. Cao, F. Peng, Y. Yang, H. Yu, Electronic synergism of pyridinic- and graphitic-nitrogen on N-doped carbons for the oxygen reduction reaction, Chem. Sci. 10 (2019) 1589–1596. https://doi.org/10.1039/C8SC04596H.
[56] Y.-X. Chen, S.-P. Chen, Q.-S. Chen, Z.-Y. Zhou, S.-G. Sun, Electrochemical preparation of iron cuboid nanoparticles and their catalytic properties for nitrite reduction, Electrochim. Acta 53 (2008) 6938–6943. https://doi.org/10.1016/j.electacta.2008.02.024.
[57] A.J. Bard, L.R. Faulkner, Electrochemical methods: fundamentals and applications, wiley New York, 1980.
[58] R.E. Davis, G.L. Horvath, C.W. Tobias, The solubility and diffusion coefficient of oxygen in potassium hydroxide solutions, Electrochim. Acta 12 (1967) 287–297. https://doi.org/10.1016/0013-4686(67)80007-0.
[59] D.R. Lide, *CRC* Handbook of Chemistry and Physics, 82nd ed., CRC Press, Boca Raton, 2001.
[60] S. Gottesfeld, I. D. Raistrick, S. Srinivasan, Oxygen Reduction Kinetics on a Platinum RDE Coated with a Recast Nafion Film, J. Electrochem. Soc. 134 (1987) 1455. https://doi.org/10.1149/1.2100689.
[61] M. Mooste, E. Kibena-Põldsepp, L. Matisen, M. Merisalu, M. Kook, V. Kisand, V. Vassiljeva, A. Krumme, V. Sammelselg, K. Tammeveski, Oxygen Reduction on Catalysts Prepared by Pyrolysis of Electrospun Styrene–Acrylonitrile Copolymer and Multi-walled Carbon Nanotube Composite Fibres, Catal. Lett. 148 (2018) 1815–1826. https://doi.org/10.1007/s10562-018-2392-6.

[62] M. Mooste, E. Kibena-Põldsepp, V. Vassiljeva, M. Merisalu, M. Kook, A. Treshchalov, V. Kisand, M. Uibu, A. Krumme, V. Sammelselg, K. Tammeveski, Electrocatalysts for oxygen reduction reaction based on electrospun polyacrylonitrile, styrene–acrylonitrile copolymer and carbon nanotube composite fibres, J. Mater. Sci. 54 (2019) 11618–11634. https://doi.org/10.1007/s10853-019-03725-z.

[63] S. Ratso, I. Kruusenberg, M. Käärik, M. Kook, R. Saar, P. Kanninen, T. Kallio, J. Leis, K. Tammeveski, Transition metal-nitrogen co-doped carbide-derived carbon catalysts for oxygen reduction reaction in alkaline direct methanol fuel cell, Appl. Catal. B-Environ. 219 (2017) 276–286. https://doi.org/10.1016/j.apcatb.2017.07.036.

[64] U. Tylus, Q. Jia, K. Strickland, N. Ramaswamy, A. Serov, P. Atanassov, S. Mukerjee, Elucidating Oxygen Reduction Active Sites in Pyrolyzed Metal–Nitrogen Coordinated Non-Precious-Metal Electrocatalyst Systems, J. Phys. Chem. C 118 (2014) 8999–9008. https://doi.org/10.1021/jp500781v.

[65] S. Yasuda, Y. Uchibori, M. Wakeshima, Y. Hinatsu, H. Ogawa, M. Yano, H. Asaoka, Enhancement of Fe–N–C carbon catalyst activity for the oxygen reduction reaction: effective increment of active sites by a short and repeated heating process, RSC Adv. 8 (2018) 37600–37605. https://doi.org/10.1039/C8RA08359B.

[66] K. Wan, Z. Yu, X. Li, M. Liu, G. Yang, J. Piao, Z. Liang, pH Effect on Electrochemistry of Nitrogen-Doped Carbon Catalyst for Oxygen Reduction Reaction, ACS Catal. 5 (2015) 4325–4332. https://doi.org/10.1021/acscatal.5b01089.

[67] K. Singh, F. Razmjooei, J.-S. Yu, Active sites and factors influencing them for efficient oxygen reduction reaction in metal-N coordinated pyrolyzed and non-pyrolyzed catalysts: a review, J. Mater. Chem. A 5 (2017) 20095–20119. https://doi.org/10.1039/C7TA05222G.

[68] J.H. Zagal, M.T.M. Koper, Reactivity Descriptors for the Activity of Molecular MN_4 Catalysts for the Oxygen Reduction Reaction, Angew. Chem. Int. Ed. 55 (2016) 14510–14521. https://doi.org/10.1002/anie.201604311.

[69] K. Ping, A. Braschinsky, M. Alam, R. Bhadoria, V. Mikli, A. Mere, J. Aruväli, P. Paiste, S. Vlassov, M. Kook, M. Rähn, V. Sammelselg, K. Tammeveski, N. Kongi, P. Starkov, Fused Hybrid Linkers for Metal–Organic Framework-Derived Bifunctional Oxygen Electrocatalysts, ACS Appl. Energy Mater. 3 (2020) 152–157. https://doi.org/10.1021/acsaem.9b02039.

ACKNOWLEDGEMENTS

I would like to express my sincere gratitude and appreciation to my supervisor Dr. Marek Mooste for the willingness to help, for taking the time to share the knowledge with me and providing continuous insightful guidance and advice throughout this research and not only. I am thankful for the experience I have received while working under his supervision.

I wish to thank Dr. Kaido Tammeveski for the support and the opportunity of letting me conduct this research.

I wish to send my gratitude to the researchers at the Institute of Physics, University of Tartu for their contribution to this bachelor's thesis.

Appendix

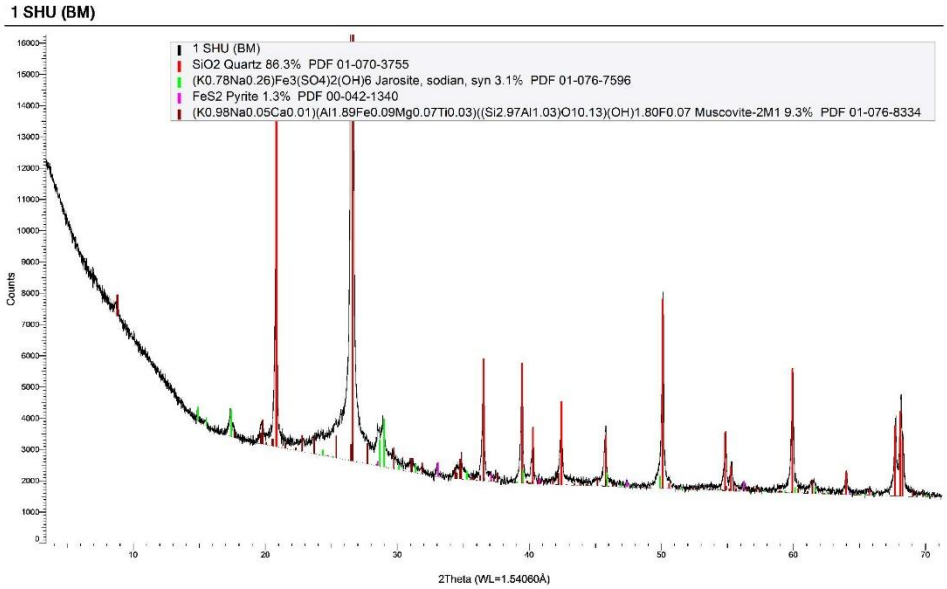

Figure S1. XRD spectra of SHUa material.

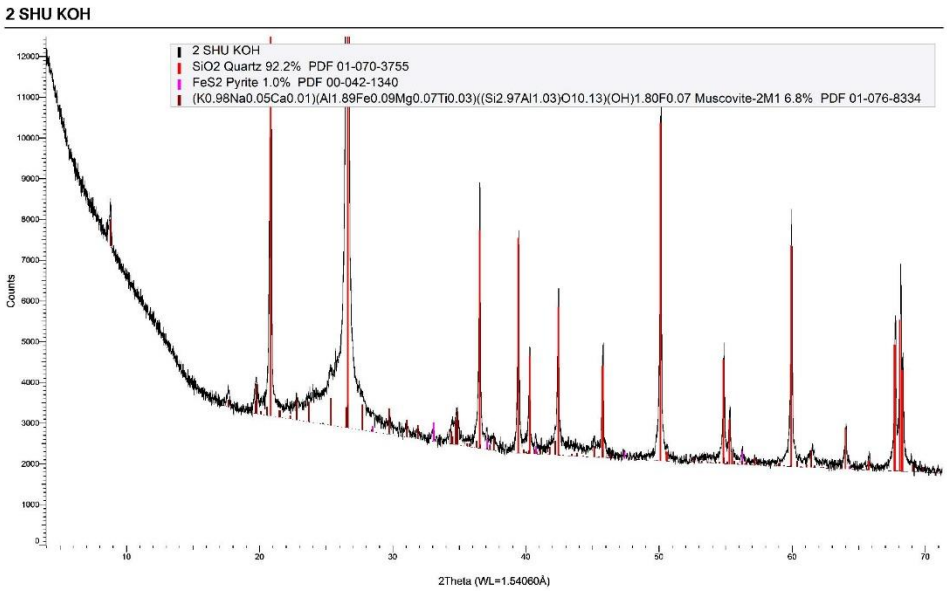

Figure S2. XRD spectra of SHUb material.

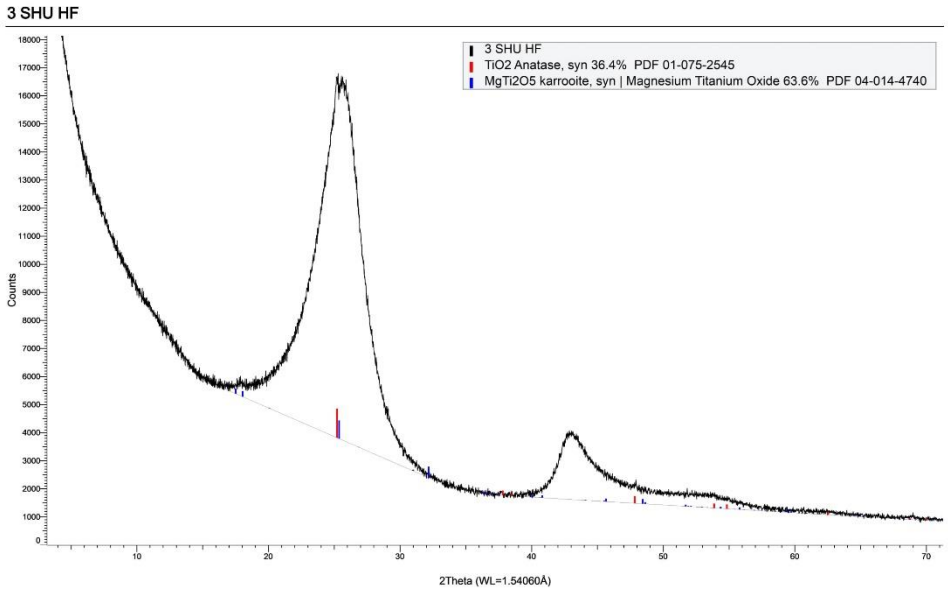

Figure S3. XRD spectra of SHUc material.

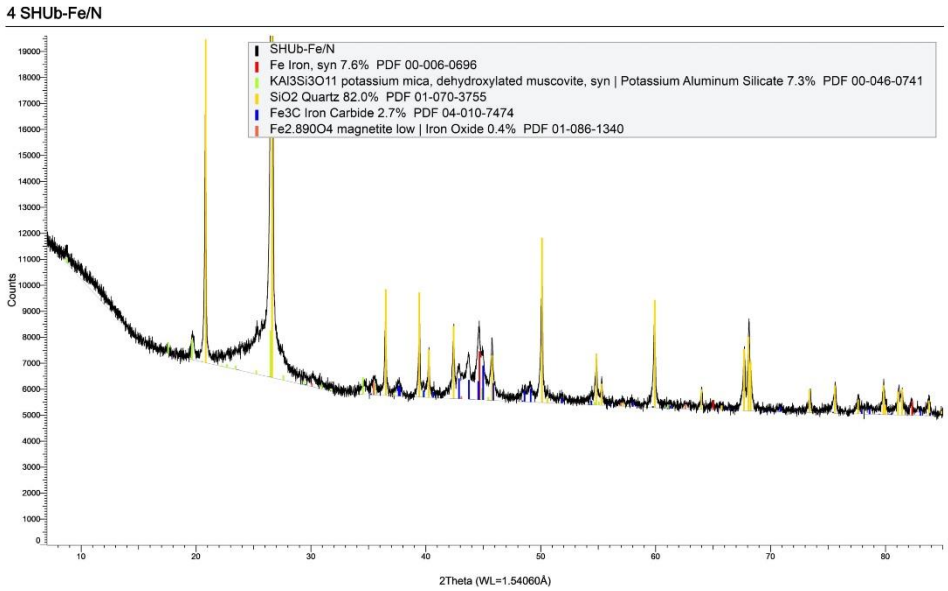

Figure S4. XRD spectra of SHUb-Fe/N material.

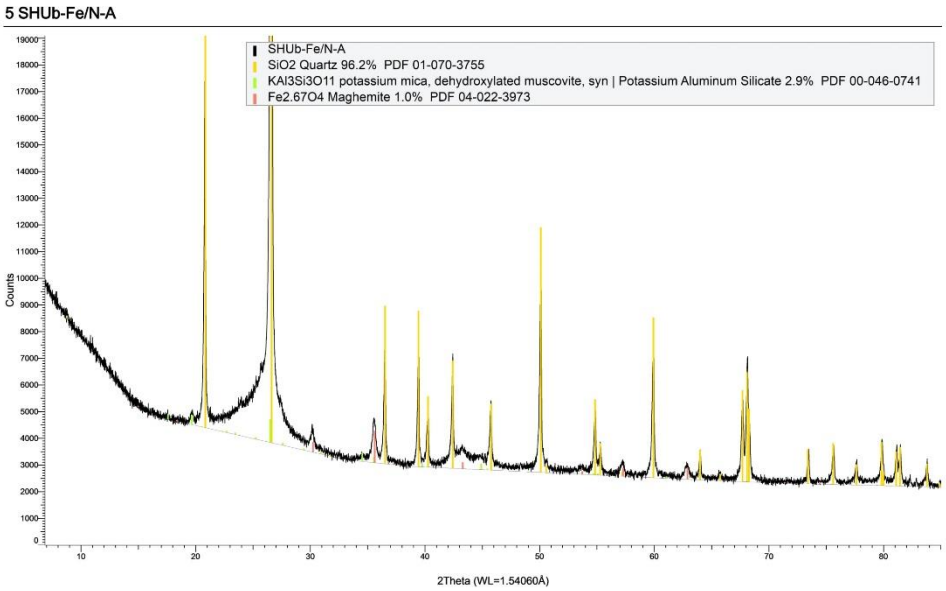

Figure S5. XRD spectra of SHUb-Fe/N-A material.

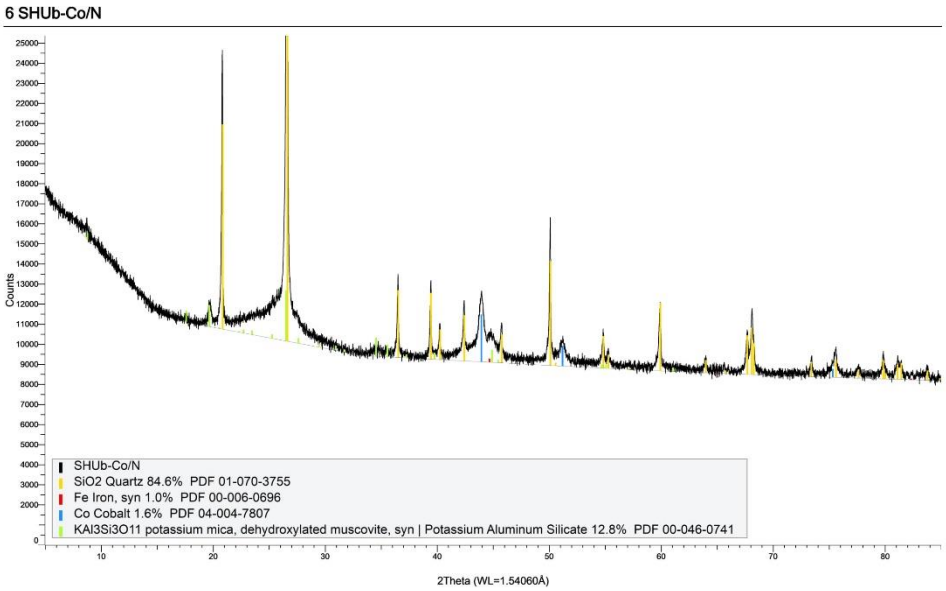

Figure S6. XRD spectra of SHUb-Co/N material.

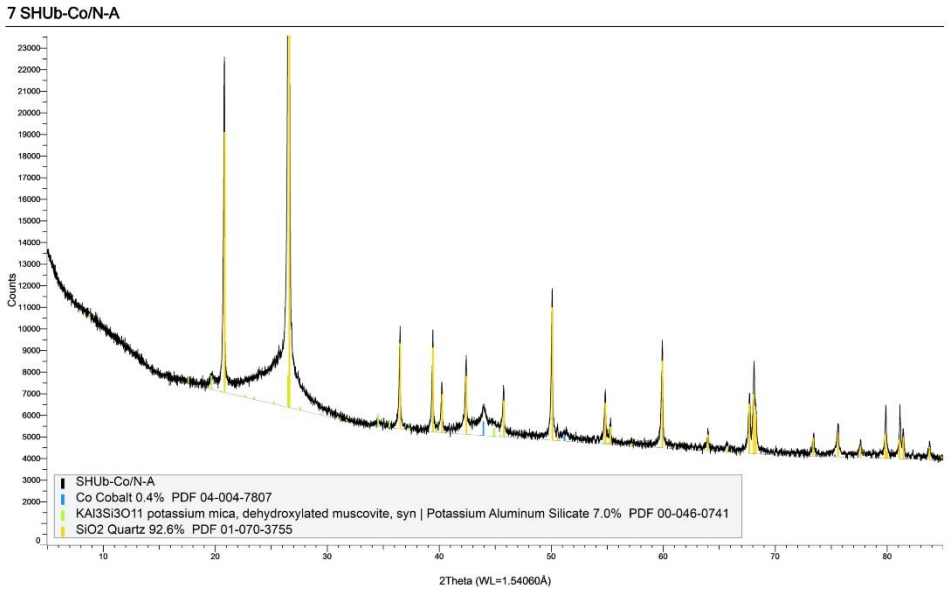

Figure S7. XRD spectra of SHUb-Co/N-A material.

NON-EXCLUSIVE LICENCE TO REPRODUCE THESIS AND MAKE THESIS PUBLIC

I, Tinatin Tkesheliadze,

1. herewith grant the University of Tartu a free permit (non-exclusive licence) to

reproduce, for the purpose of preservation, including for adding to the DSpace digital archives until the expiry of the term of copyright, Oxygen Reduction Catalysts Based on Iron and Cobalt phthalocyanine Modified Shungite,

supervised by Dr. Marek Mooste and Dr. Kaido Tammeveski,

2. I grant the University of Tartu a permit to make the work specified in p. 1 available to the public via the web environment of the University of Tartu, including via the DSpace digital archives, under the Creative Commons licence CC BY NC ND 3.0, which allows, by giving appropriate credit to the author, to reproduce, distribute the work and communicate it to the public, and prohibits the creation of derivative works and any commercial use of the work until the expiry of the term of copyright.

3. I am aware of the fact that the author retains the rights specified in p. 1 and 2.

4. I certify that granting the non-exclusive licence does not infringe other persons' intellectual property rights or rights arising from the personal data protection legislation.

Tinatin Tkesheliadze

20/05/2020